interference

in

RANDOM LASERS

thesis eigen werk 4 - frank j. poelwijk

universiteit van amsterdam 2000

research carried out at the

van der waals-zeeman laboratory

faculteit der wiskunde, informatica, natuur- en sterrenkunde

universiteit van amsterdam

valckenierstraat 65, 1018 xe amsterdam

supervisors:

gijs van soest

prof. dr. ad lagendijk

no gain, no pain...

c o n t e n t s

prologue

In the period following the first description of a laser in 1958 [1] interest was raised for systems that did not get their feedback by a mirror cavity but by scattering off a rough surface. From the first theoretical calculations [2] it was evident that light coming from these systems shows some properties resembling those of a cavity laser, although the generative mechanisms are quite different. Because of military interest, particularly in the Sovjet Union, the subject disappeared from the usual research programmes, only to return about fifteen years later, due to the renewed interest in light diffusion in the mid-eighties (e.g. localization of light, enhanced backscattering). In articles of Lagendijk and Wiersma [3, 4] scattering amplifying media were given their now familiar name: *random lasers*.

In order to build a random laser, nothing more is needed than a fluorescent material in which light will make a random walk. The recipe thus consists of two ingredients: amplification and multiple scattering of light.

Random lasers have been investigated in the form of ground laser-crystals where the amplifying grains also provide the scattering. Other measurements have been performed on silica spheres with built-in laser dye molecules and recently there have even been reports of random lasing dye-doped fruit and vegetables. In our experiments we use a straightforward realization of a random laser: a solvent with a laser dye to provide the amplification and suspended TiO_2 particles to do the scattering. An additional benefit is that the scattering and amplification are separated so that they can be treated as independent variables. Although the sample preparation may be simple, the observable effects are diverse and their quantitative description is usually rather involved.

One of the characteristics of laser action that is also exhibited by a random laser is the presence of a laser threshold. Upon increasing the number of excited atoms or molecules in a conventional laser system spontaneously emitted

light experiences more and more gain by stimulated emission. At some point the gain is large enough to compensate for the losses and the system is able to amplify light. This point is associated with the threshold of a laser system. Since the amount of gain and loss in the system in general is frequency dependent, there is some limited frequency interval that reaches the threshold first and this light consumes most of the gain in the active medium. As a result of this the output power in the considered spectral region suddenly increases and the output spectrum becomes narrower.

In a conventional laser, such as a Fabry-Perot oscillator with an amplification medium in between the two mirrors, the spectral selection mechanism is very specific: the lasing mode is selected by being in resonance within the Fabry-Perot system and the spectrum can become very narrow. In the random laser case however, there is no preferred resonance distance to do the same sort of selection. Here the narrowing of the spectrum takes place around the modes in the dye spectrum which have the most favorable combination of a low absorption and a high stimulated emission efficiency.

There have been experiments on scattering gain media in which the presence of an intense probe beam forced the spectral collapse to center around the wavelength of that beam, the so-called *injection locking* [5]. The probe beam depletes all the gain and the output is spectrally very narrow. Other experiments show that fluorescence pulses get shortened in the medium upon increasing pump energy [6, 7]. In the meantime people are looking for applications of random lasing materials. Very bright high-definition displays and medical imaging are some of the most mentioned, but all still to be developed.

One approach to random lasers is that from the viewpoint of an 'ordinary' laser, describing it in terms of e.g. feedback mechanisms, output coherence and efficiency and trying to see how far the parallels can be extended. Seen in this way we can consider a random laser as one of the many variations that stretched the definition of a laser beyond the narrow limits of 'a system with two mirrors and a gain medium in between'.

In this thesis we do not follow this approach, which sometimes tends to lean towards the side of definitions. The goal of our research is investigating the properties of a multiply scattering system as they are modified by the introduction of light amplification. We are not so much trying to settle the question whether what we or other people are looking at is a *true* random laser.

Chapter 1 states the basic theory that is involved in our optical experiments. A brief overview of light diffusion and laser action is given. More details, needed to account for the experimental data, are set out at the beginning of each of the subsequent chapters about the different experiments we performed.

The first of these experimental chapters, chapter 2, is about our measurements of dye spectra, the influence of adding scatterers and the threshold behaviour of an optically pumped dye-scatterers system. These are preparatory measurements by which different combinations of dyes and solvents are characterized in order to choose the right samples for our later experiments.

In chapter 3 experiments on speckle statistics are presented. We have measured spatial correlations of speckle and intensity statistics of the dye-scatterers system as a function of pump and probe beam intensities.

The most important part of our experiments is found in chapter 4, where we present measurements of enhanced backscattering on amplifying media. These measurements are of particular interest, since they probe the light paths through the system and hold information about a wide range of relevant physical quantities, such as the transport mean free path and the degree and distribution of inversion in the samples.

1 theory of light scattering and lasing

Light that propagates through vacuum travels along straight lines. When light travels through some medium consisting of atoms or molecules, its electric field acts as a driving force on the charges that are present in the medium. These charges are forced to oscillate and the accelerated charges thereupon emit light themselves. Moving charges emit light in all directions except for that in which they move. By this mechanism light traveling through a medium can in principle alter its direction of propagation, but because of symmetry this will not happen if the medium is homogeneous. Only when the resonance properties of the atoms exhibit a spatial variation, which is expressed by a varying index of refraction $m(\vec{r}, \omega)$, there is a possibility of changing the direction of the light. Depending on the length scale of the variations we call this directional change scattering (at small length scales) or refraction (at larger length scales).

Just as in a classical oscillator, the motion of the driven particles can lead to the dissipation of energy. This results in the decrease of the intensity of the incoming light, the extent of which is expressed by the absorption coefficient $\kappa(\vec{r}, \omega)$. This coefficient determines how much of the initial energy is converted into other forms of energy, e.g. vibrations of molecules or excited electron states. If a light beam is incident on a medium, scattering and absorption together determine the extinction, i.e. the amount of light taken out of it in the forward direction.

1.1 single light scattering

The description of reflection, by means of Snell's law, is very simple, because we are in the limit where we can consider the media in which the light propagates as a continuum. Describing scattering phenomena is harder because we have to look explicitly at a microscopic level. In the case of our experiments we have scattering TiO_2-particles with an average diameter of about 200 nm, which

is of the same order as the wavelength of visible light. In determining the scattering properties (angular intensity distributions as a function of incoming angle, frequency or polarization) of one particle we have to account for its exact shape. Calculations of this sort have been done analytically only for some simple shapes: spheres (Mie theory, see a.o. [8]), ellipsoids and cylinders. When light is scattered by an irregularly shaped particle, calculations get very involved and have to be solved numerically.

If the light is incident on a large collection of these particles, things get somewhat simpler, because the random shape variations average out and we can obtain information the mean particle size and the overall shape (static light scattering, see a.o. [8]). On the other hand, because of the wave character of light, light scattered from different particles interferes. In this way singly scattered light from a collection of particles echoes the structural properties of the investigated sample (static and dynamic light scattering, [8, 9]).

1.2 multiple light scattering and diffusion

At a still higher number of particles in the sample or at larger sample dimensions, we expect light to scatter more than once before leaving the scattering volume. This can also be accomplished by increasing the refractive index contrast between the scattering particles and the suspending liquid. We now enter the multiple scattering regime. Interference effects are scrambled due to the many random scattering events[1] and light is assumed to propagate diffusely. That is to say that we can describe the propagation of the light by the diffusion equation for particles in a medium, which is also commonly known as the *heat equation*

$$\frac{\partial n(\vec{r},t)}{\partial t} = D\ \nabla^2 n(\vec{r},t) \tag{1.1}$$

where $n(\vec{r},t)$ is the particle concentration at a point in space $\vec{r}$ and at a time t. D is the diffusion constant representing the speed of the diffusion process. This equation holds when there is no dissipation or generation of light in the sample, because only in this way the situation can be analogous to particle diffusion. In a way the fact that light diffusion can be modeled by particle diffusion seems rather odd when the wave nature of the light is considered. Experimentally though, it is found that the diffusion approximation is rather good when compared with the more exact transport theory (for a comparison: see [10]).

[1] Some specific interference effects, however, will persist in the diffuse regime, like enhanced backscattering. We will come to this in chapter 4

The distinction between the single and multiple light scattering regimes can be made in a rather simple way by measuring the transmission of light through a scattering sample as a function of its thickness. In the single scattering limit chances for light being scattered in the exact forward direction are very low and we can consider all scattered light as being lost for the ongoing beam. Considering non-absorbing scattering samples we find the incident intensity decreasing as $e^{-\alpha L}$, with α being some proportionality constant and L the sample thickness. This relation is also known as the law of Lambert-Beer for a beam through a non-scattering absorbing medium. In the case of multiple light scattering, light is diffuse and there is no ongoing beam present. If we compare the incoming intensity and the diffuse intensity at the back side of the sample (integrated over all directions), we find a $1/L$-behaviour [11].

1.3 cross-sections and mean-free-paths

The chance of light interacting in some way with a particle is expressed by the cross-section, $\sigma(\omega)$, for the relevant type of interaction, for example scattering or absorption. The cross-section usually depends on the frequency of the light ω ($= 2\pi f$). The total chance of interacting depends on the density of particles in the medium n.

With these notions we can introduce a very useful concept in scattering theory, the mean-free-path, being $\ell = \frac{1}{n\sigma}$. The mean-free-path is a measure for the average distance between two events, for example in the case of scattering. Or it is a characteristic distance scale at which the relevant quantity produces its effect, for example in the case of absorption where the inelastic mean-free-path gives the distance light has to travel in an absorbing medium in order to be reduced to $\frac{1}{e}$ of its initial value.

Througout this thesis the following mean-free-paths are frequently used:

the scattering mean-free-path $\ell_s = \frac{1}{n\sigma_s}$

the transport mean-free-path $\ell_t = \frac{1}{1-<\cos\vartheta>}\frac{1}{n\sigma_s}$

which gives the average distance at which the propagation direction of the light is randomized. $<\cos\vartheta>$ is the average cosine of the scattering angle for each scattering event. In the case of isotropic scattering ℓ_t is equal to ℓ_s. Because ℓ_t is usually the more physically relevant of the mean-free-paths associated with scattering, we will drop the subscript and write ℓ instead.

We can identify the single and multiple scattering regimes described earlier by comparing the sample dimensions, for example the sample thickness L, with the scattering mean-free-path ℓ_s. In the case $L \ll \ell_s$ we are in the single scattering limit, which means that higher order scattering events can be neglected. In the case $L \gg \ell_s$ we have multiple scattering.

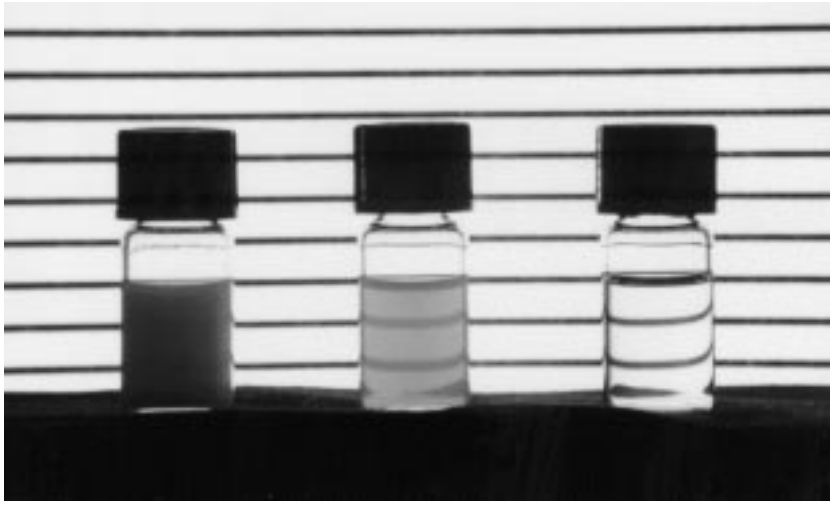

figure 1.1 *Three samples demonstrating the different scattering regimes. On the left we have* $\ell_s = \frac{L}{10}$*, in the middle* $\ell_s = L$ *and on the right* $\ell_s = 10L$*. The samples are illuminated from the back.*

the inelastic mean-free-path $\ell_i = \frac{1}{n\sigma_i}$

the diffusive absorption length $L_a = \sqrt{\frac{\ell\ell_i}{3}}$

which are important in absorbing systems. ℓ_i is the length of the light path in which the intensity is reduced to $\frac{1}{e}$ of its initial value and L_a gives the average distance between begin and end points of paths of length ℓ_i [10].

the mean-free-path for gain $\ell_g = \frac{1}{n\sigma_g}$

the diffusive amplification length $L_g = \sqrt{\frac{\ell\ell_g}{3}}$

which are the analogs of ℓ_i and L_a for amplifying systems.

1.4 light amplification

As was mentioned in the prologue we have to introduce amplification of light in addition to scattering in order to realize a random laser. Light can be amplified by using a medium containing atoms or molecules that can be brought into an excited state. In a radiation field an excited molecule or atom cannot only emit light spontaneously, but also be stimulated by a photon to decay and thereby radiate a photon of the same energy, direction and phase-relation as the stimulating photon (figure 1.2).

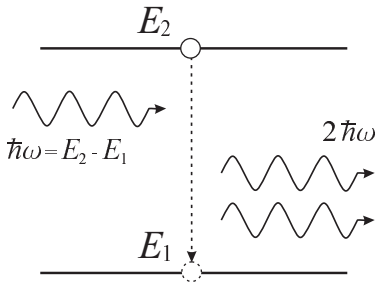

figure 1.2 *The scheme of stimulated emission. A photon with energy $\hbar\omega$ makes an excited atom emit a photon of the same energy, direction and phase relation. Stimulated emission only takes place when the energy of the stimulating photon corresponds to the difference between energy levels of the excited atom.*

For this situation we can formulate equations for the rate of change of the number of atoms or molecules in the excited state N_2, and the number of atoms in the de-excited state N_1 (see for example [12]), due to absorption, spontaneous and stimulated emission

$$\frac{\mathrm{d}N_1}{\mathrm{d}t} = -\frac{\mathrm{d}N_2}{\mathrm{d}t} = N_2 A + (N_2 - N_1) B \bar{W} \tag{1.2}$$

$\bar{W}$ is the mean energy density of the radiation and A and B are the Einstein-coefficients expressing the probability per unit time for spontaneous emission and that for absorption and stimulated emission respectively.

Now assuming a non-scattering medium where the light propagates along the direction of the z-axis and considering the equilibrium situation, we can infer from the rate equations (see again [12]), that

$$\frac{\partial I}{\partial z} \propto -(N_1 - N_2) B I \tag{1.3}$$

where I is the intensity of the light beam of a certain frequency at a certain depth z in the sample. It should be noted that the solution of this is not simply a negative exponent, since the numbers N_1 and N_2 depend on I via the energy

density $\bar{W}$. Now, for $\frac{\partial I}{\partial z} > 0$ we have amplification of light in the direction of the incident beam. From this we can see that we should have $N_2 > N_1$, the condition we call population inversion. But we seem to have a problem since in a system with two energy levels it is impossible to achieve inversion. We can understand this by considering that at $N_2 = N_1$ every photon of the incident beam has an equal chance of exciting or de-exciting a molecule of atom and that if N_2 would be larger than N_1 the chance of de-exciting is larger and N_2 would immediately decrease.

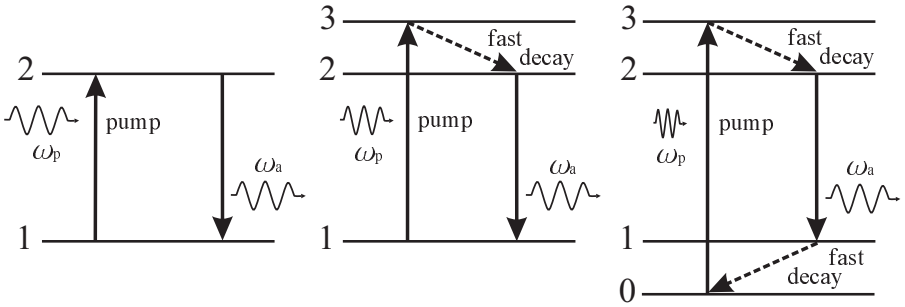

figure 1.3 *Different configurations of the energy levels of atoms or molecules. On the left is the two-level system, which is unable to provide amplification, because the pumping photons have the same frequency as the photons created by stimulated emission. In the three-level system the pumping photons are not resonant with the transition between levels 1 and 2, so that N_2 can become larger than N_1 and light amplification becomes possible. The same holds for the four-level system. Here the amplification process is still more efficient, because amplified photons cannot be reabsorbed.*

This problem can be overcome by using a three-level system (figure 1.3), where there is a third state to which the atoms or molecules are excited. This third state should then decay very fast to the second state, associated with N_2 in the considerations above. The frequency of the exciting photons is no longer resonant with the de-excitation, or the stimulated emission and in this way it *is* possible to get $N_2 > N_1$. What is needed for operating such a system is a 'pump' source of frequency ω_p to amplify light with frequency ω_a and where $\omega_p > \omega_a$.

This process can still be made more efficient if the first level (associated with N_1 above) also has a low stability (figure 1.3). Atoms or molecules from the first state decay fast to their ground state. Since N_1 is nearly zero, reabsorption of the light to be amplified (with frequency ω_a that could excite the atoms or molecules from their first level to their second level) is prevented.

From a practical point of view things are somewhat more complicated. In molecules there are usually many energy levels present, so there can be many of

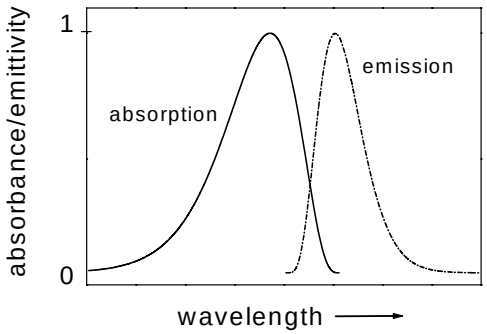

figure 1.4 *Typical absorption and emission cross-sections for a laser dye, as a function of the wavelength of the light. The dashed line is the emission cross-section, the solid line is the cross-section for absorption. Usually the two profiles overlap.*

these schemes active within one amplifying medium. Added to this is the fact that the transitions are not sharply defined due to broadening mechanisms. In a typical gain medium, like the *laser dyes* we use in our experiment (which in principle are 4-level systems), all this results in a broad absorption band (in the order of tens of nanometers) and a broad emission band (of the same order of width) which usually have some overlap (figure 1.4). Because of the presence of this overlap, light that is emitted on the blue end of the emission profile has a chance to be reabsorbed. This chance increases when the dye concentration is increased or, as we will see later, when scatterers are introduced in the dye solution. The dyes we use, like Coumarin 6 and Rhodamine 110, are large molecules (around 400 atomic mass units) with several aromatic groups [13].

1.5 laser action and the threshold condition

In a realistic system set up for light amplification we do not always get an appreciable contribution of stimulated emission, since a part of the generated light is lost by means of reabsorption or just by leaving the amplification medium before it is able to stimulate the decay of other atoms or molecules.

Whether we have amplification is determined by the so-called *threshold condition*: gain equals loss in a certain system. For example, if we want to amplify a light beam, we have to account for the losses the incident beam suffers. Losses can be due to absorption followed by non-radiative decay or by spontaneous emission, which is isotropic and therefore will not contribute to the beam intensity. To get amplification of the beam, we have to see to it that the pumping rate at which energy is supplied to the system, is larger than the loss rate.

What we observe at low pumping powers (low inversion ratio) is just fluorescence of the gain medium due to the spontaneous decay of the excited atoms or molecules. At higher pumping powers, when there are more atoms or molecules excited, spontaneously emitted photons cause stimulated emission of other photons. This is called *amplified spontaneous emission* (ASE). ASE is stronger when more inversion is present and so the intensity is the highest in the direction of the largest elongation of the amplifying volume. At high pumping powers, ASE light will form a more or less directed beam which has a degree of spatial coherence depending on the sample size. Because of stimulated emission, emission lifetimes in ASE light are shorter compared to normal fluorescence lifetimes (see for example [7]). Another notable effect of ASE light is the spectral narrowness of the light compared to the unamplified fluorescence spectrum. This is caused by the wavelength dependence of the amplification efficiency of the laser medium. Details of this mechanism which is called *gain narrowing* will be discussed in chapter 2.

When an amplifying medium is placed between two parallel mirrors, reflection makes that almost no light is lost in the direction perpendicular to the mirrors. Light that has once been emitted is reflected by the mirrors and can pass several times through the amplification medium. This mechanism is referred to as *feedback*. A standing wave can arise for wavelengths being an integer fraction of the distance between the mirrors. The specificity of the wavelength selection depends on the quality factor Q of the mirror cavity, which is determined by the reflectivity of the mirrors. When one of the mirrors is slightly transmittent, a part of the amplified light comes out at that side as a spatially and temporally coherent beam. What is described here is a simple model of a cavity laser (light amplification by stimulated emission of radiation). Laser light can reach a very high temporal (longitudinal) coherence. For certain systems coherence lengths of hundreds of meters can be reached.

In a laser system the threshold is very important. In a cavity laser all light that is not emitted in the direction perpendicular to the mirrors is lost. Also light that is transmitted through one of the mirrors (which is essential, since this provides the output) should be incorporated in the loss-term. When the pumping rate is high enough to compensate for this loss, a number of very characteristic changes in the properties of the light inside the cavity will occur.

There will be an almost total collapse of the spectrum of the laser light (figure 1.5a). Depending on the quality of the cavity the linewidth $\frac{\Delta\lambda}{\lambda}$ of laser emission can easily reach values of the order of 10^{-5}. Because of this spectral collapse a sudden increase in output intensity is observable when the threshold is crossed (figure 1.5b).

The statistics of the emitted light are also changed when the threshold is crossed. If we look at the mean number of photons leaving the cavity, we

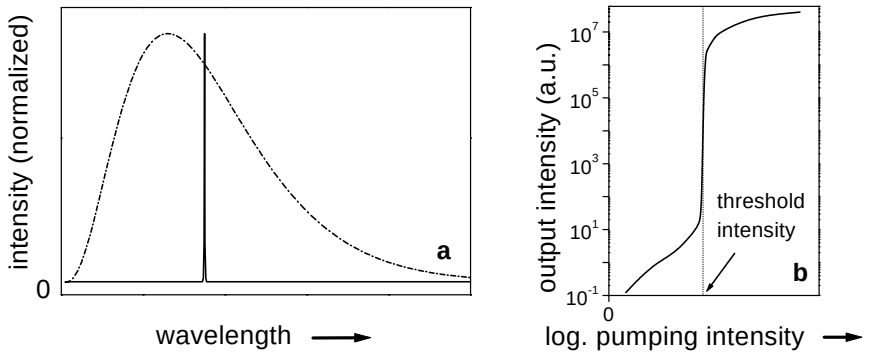

figure 1.5 *a) The emission spectum of an amplification medium. The dashed line is the normal fluorescence spectrum and the solid line is the collapsed spectrum when the medium is used in a laser system. b) Output intensity (mean number of photons per unit time leaving the cavity) of a single mode laser as a function of pumping energy (after Loudon, [12]). When the threshold is crossed, the output energy increases very fast.*

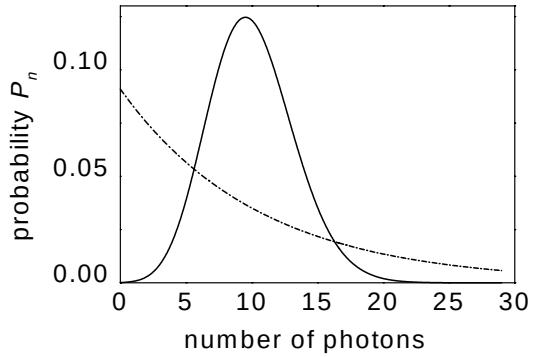

figure 1.6 *Distributions of the number of photons leaving a laser cavity per unit time. The dashed line corresponds to the situation below threshold and the solid line to that well above threshold. Both distributions are plotted for a mean number of photons, $\bar{n}$ of 10.*

observe a certain distribution

$$P_n = \frac{\bar{n}^n}{(1+\bar{n})^{1+n}} \tag{1.4}$$

(where $\bar{n}$ is the mean number of photons, being a function of the pumping rate) below threshold, and a Poisson distribution

$$P_n = \frac{\bar{n}^n \mathrm{e}^{-\bar{n}}}{n!} \tag{1.5}$$

above threshold (see [12]).

1.6 random lasers

A random laser combines amplification with scattering of light. On one hand these systems have properties similar to ordinary lasers, like the narrowing of the spectrum and the presence of a threshold in the output energy (as will be investigated in chapter 2). We will investigate if statistical properties of random laser light are changed under the influence of threshold crossing in chapter 3. On the other hand random lasers can be viewed as multiple scattering systems in which the propagation of light is highly affected by the presence of gain. Amplification will change the distribution of path lengths along which light travels in the system: when inversion is present, light making long paths through the medium will be amplified more than light making short paths. A means to investigate the change in path length distribution is the study of enhanced backscattering cones. This approach is taken in chapter 4.

2 spectra and thresholds

One of the most noticeable properties of a random laser is the narrowing of the frequency spectrum of the emitted light. When we excite the amplifying medium of a random laser by pumping it in its absorption band, we observe a broad fluorescence spectrum which will get narrower if the pumping intensity is increased. Besides on pumping intensity, the so-called *gain narrowing* effect is dependent on a number of parameters like the absorption and transport mean free paths [14], the dimensions of the gain volume [15] and the gain length. This will make the underlying dynamics more complicated than those of spectral narrowing in a conventional laser. The concept of a laser threshold, known from conventional lasers, is also transferred to random lasers, but this too will turn out to be more complex. In this chapter we will focus on the spectral features of the light emitted by random lasers. Samples are characterized for use in the experiments of chapters 3 and 4.

2.1 theory of spectral narrowing and peak shift

If inversion is present in a medium, spontaneously emitted light can be amplified by stimulated emission, as we saw in the previous chapter. Gain narrowing was said to occur if the share of stimulated emission is large enough. In the case of a transparant gain medium it is easy for light to leave the pumped volume, so there must be an appreciable inversion to observe spectral narrowing effects. If we can 'reuse' the emitted light to stimulate other atoms or molecules to decay (*feedback*), the effects under consideration will occur at lower pumping intensities and usually in a much more pronounced fashion. In a conventional laser system emitted light is reintroduced to the amplification medium by reflections from the mirrors of the cavity. In a random laser feedback is realized by scattering from random variation of the index of refraction. Light in these systems will make a random walk so that it travels longer distances in the gain volume and more stimulated emission can occur.

The first treatment of gain narrowing in a random scattering system is given by Letokhov [2, 16], only a few years after the first theoretical discussion of a cavity laser by Schawlow and Townes [1].

We will now discuss a simple picture highlighting the essence of gain narrowing. More detailed and quantitative descriptions of the dynamics of random lasers are to be found in [17] or [18].

At low pumping powers, the inversion of the amplification medium of the random laser is low and we can assume all atoms or molecules to decay by spontaneous emission. We observe a broad fluorescence spectrum $F(\lambda)$, which is a direct measure for the wavelength dependent cross section of spontaneous emission $\sigma_{\mathrm{s}}(\lambda)$. At higher pumping rates, inversion gets larger and spontaneously emitted light is amplified by stimulated emission (amplified spontaneous emission, or ASE, see previous chapter). The amount of amplification a photon receives, is proportional to the factor $\gamma(\lambda) = \mathrm{e}^{l/\ell_{\mathrm{g}}(\lambda)}$, which depends on the quotient of the travelled path length l and the gain length or gain mean free path ℓ_{g}. When the path length l is equal to ℓ_{g}, light is amplified by a factor e. The amplification factor γ is a function of wavelength. As we have seen in section 1.3, $\ell_{\mathrm{g}} = \frac{1}{n\sigma_{\mathrm{g}}}$ and the amplification factor can be rewritten as

$$\gamma(\lambda) = \mathrm{e}^{l\, n\, \sigma_g(\lambda)} \tag{2.1}$$

where σ_{g} is the cross section for stimulared emission and n is the density of inverted atoms or molecules. We will say something more about the wavelength dependence of σ_{g} later. In the case that stimulated emission is dominant over spontaneous emission, the value of the amplification factor γ for a certain

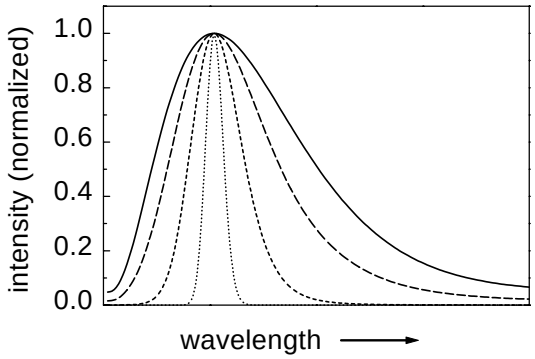

figure 2.1 *Demonstration of the gain narrowing effect. The solid line represents the spontaneous emission spectrum from an amplification medium. The dashed lines (with decreasing dash length) represent the emission spectrum for increasing values of the inversion density n. All curves are normalized to 1.*

frequency is a measure for the relative importance of that frequency in the total emission spectrum, and it follows that the emission spectrum itself is proportional to the amplification factor $\gamma(\lambda)$. Knowing that the stimulated emission cross section is approximately proportional the spontaneous emission spectrum ([12], when the wavelength interval over which they are compared is not too large), we can just put the fluorescence spectrum in the exponent of the γ factor and monitor the spectral narrowing by plotting the wavelength dependent γ for different values of the inversion density n, thus for different pumping energies (as is done in figure 2.1).

When measurements are done on random lasers, not only a narrowing of the spectrum is observed, but usually also a shift of the maximum of the emission profile. This can have two causes. Firstly, the spontaneous emission spectrum and the cross section for stimulated emission do not have their maxima at the same frequency. By this cause, the emission maximum can shift to the blue as well as to the red. Secondly, particularly when laser dyes are used as gain medium, emitted light can be reabsorbed. Since the absorption and emission cross sections of a laser dye usually overlap (see figure 1.4), light from the blue end has a higher chance of being absorbed than light from the red end and this will tend to shift the emission spectrum towards the red. This effect will become more important if the dye solution gets more concentrated, or if the light stays longer in the system, which is achieved by the introduction of more scatterers. When, conversely, the pumping intensity is increased, the dye will get saturated, the absorption will decrease and the spectrum will shift back to the blue again. Many spectral features of random lasers are listed with their explanations in [17].

2.2 threshold of a random laser

The threshold of a conventional laser system specifies the pumping intensity where the gain of light in the lasermode equals the loss. To the loss contributes light that ends up outside the lasermode (spontaneous emission, which is isotropic) as well as the light that is coupled out of the cavity by the transmitting mirror. In order to determine whether we are below or above the threshold, we can monitor an amount of light in the lasermode, 'follow' it for one round trip and see if it has decreased or increased. In the random laser case it is not trivial what loss refers to (see also [19]). Assuming that there is a negligible absorption of emitted light, it follows that for any inversion density for every possible light path through the system there is gain. Usually the position of the threshold of a random laser is determined from a measurement of the spectral narrowing effect (figure 2.2). This implies that the threshold of a random laser specifies the point that a 'reasonable' amount of stimulated

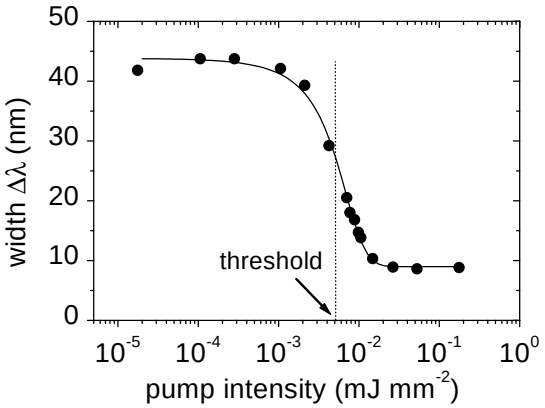

figure 2.2 *Typicical measurement of the width of the emission spectrum of a random laser as a function of pumping intensity. The picture is adapted from [15]. The threshold pumping intensity is assigned to the inflexion point of the curve.*

emission is present in the system. On a microscopic level we can now look at loss being loss from a certain volume. The threshold condition could now be associated with the point that there is more light generated in this volume than diffusing out of it. It may be clear that there will not be a well-defined pumping intensity where changes in the emission of a random laser can be expected. This in contrast to a conventional laser.

The threshold pump energy is found experimentally to depend on sample properties ℓ, L_a [14], but also on the geometrical parameters, like the diameter of the pumping beam [15], which is consistent with the considerations about the random laser threshold above. These points are elaborated upon in [19].

A consequence of the spectral narrowing is the increase of the output energy of a random laser, when we observe it in a small spectral interval around the peak wavelength of the narrowed spectrum. At low pumping energies (a broad emission spectrum) the output intensity is proportional to the pump intensity. This is not surprising because it merely states the conservation of energy. The frequency integrated spectrum is directly proportional to the pumping energy and as long as the shape of the spectrum remains constant, the output intensity of every part of the spectrum is proportional to the pumping energy. When the pump energy is increased, the spectrum will narrow and light is redistributed into the region where we are looking. So the output power will make a sudden increase. At higher energies the spectrum is not narrowing so much further, and the output intensity and the pumping energy will become proportional again.

To extract the threshold pump intensity from these data, usually the sec-

ond linear part (after the spectrum has narrowed down) is extrapolated to zero output energy. This procedure is legitimately applied to conventional lasers, but in the case of random lasers, the expected proportionality of the output intensity and pumping intensity does not seem to validate the procedure. However, since it is commonly used, we have initially done output intensity measurements and determined the threshold from them. We will present the results in the end of this chapter.

2.3 experiment

2.3.1 choosing the sample

We have decided to use high gain samples where the influences of the amplification medium and the scattering surface can be varied independently. We will take a simple broad-band amplification medium, which is widely used in laser-optics: a transparent fluid with a laser dye dissolved in it. For the scatterering we need particles having a large contrast of the index of refraction with the solvent of the laser dye (most liquids have $n = 1.3$ to 1.5), but being non-absorbant for the wavelength range we want to work in (450 to 650 nm). TiO_2 in the crystalline form of rutile with its refractive index of 2.6 and its absorption band at wavelengths lower than 400 nm will serve this purpose. The particles we use are irregularly shaped and have a diameter of 220 ± 70 nm [20]. They are obtained from the paint industry (white paint) and are coated to prevent aggregation. To be in the same scattering regime as earlier experiments we use a 1 volume-% suspension, resulting in a mean free path ℓ of about 10 μm (from measurements in [10]). The dye concentration we use is in the order of 2 mM, as prescribed by [13] to get optimum performance for dye lasers without having too much influence from quenching. This results in a ℓ_i of about 100 μm.

The lasers we will use to excite the dye molecules in our experiments of chapters 3 and 4 are pulsed. This is particularly important at higher pumping intensities, since pulsed excitation greatly reduces the number of dye molecules entering into the triplet state, i.e. excited state absorption. A large contribution of emission from triplet states would considerably alter the shape of the spectrum, which is undesirable.
We started our experiments by determining which dye-solvent combination will be the most suitable for our speckle statistics and enhanced backscattering experiments (chapters 3 and 4). Our search criterium is whether a sample has a large stimulated emission efficiency and a negligible absorption efficiency at the wavelength of the laser used to probe the samples in our later experiments. For this probe beam initially a frequency doubled Nd:YAG, 532 nm was used, later on in chapter 4 a tunable OPO (450-650 nm) turned out to be more

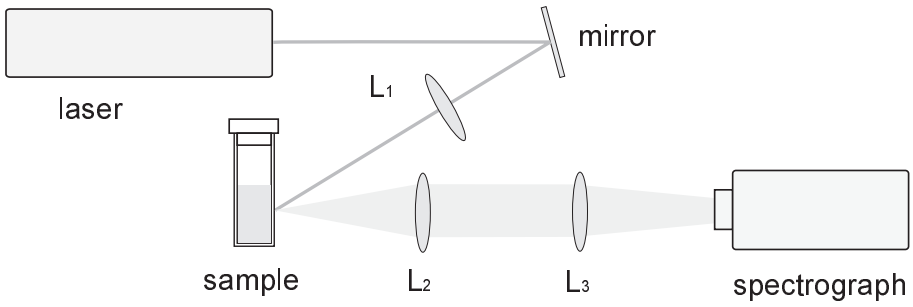

figure 2.3 *Scheme of the setup for recording the dye spectra. Depending on the type of dye a Q-switched frequency tripled Nd:YAG laser (355 nm, pulsed), an argon laser (cw at 488 nm) or a frequency doubled Nd:YAG (532 nm, pulsed) is used to excite the dye molecules. A system of lenses is inserted to increase the amount of light that reaches the spectrograph.*

suitable and in that case the wavelength can be optimized for a certain laser dye. The remaining sections of this chapter are divided in measurements on green dyes for the 532 nm probe beam and on the more commonly used red dyes to which the probe frequency can be adapted for optimum performance.

We recorded fluorescence spectra of a number of potentially usable laser dyes without TiO_2-particles. The setup is shown in figure 2.3. A laser beam is incident on the sample and the fluorescence light is collected by a system of lenses. A grating spectrograph with a photo diode array behind it form the detecting end of the setup.

green dyes

A Q-switched frequency tripled Nd:YAG (355 nm) is used to bring the green dye molecules in an excited state. As shown in figure 2.4 the Uranin dye seems to be the best candidate, because it shows the highest relative emission at 532 nm, but when TiO_2-particles are introduced we find them sedimenting very fast. Probably they are glued together by the dye. Also in other solvents (ethanol, benzylalcohol, 2-methyl-2,4-pentanediol and water) the scattering particles aggregate, which makes Uranin useless for our experiments. Rhodamine 110 is unsuitable because the absorption at 532 nm is rather large (see [13]). Therefore Coumarin 6 is used in measurements in which a the probing laser is a doubled Nd:YAG. As a solvent we make use of the higher viscosity fluids benzylalcohol (BzOH) and 2-methyl-2,4-pentanediol ($Pm(OH)_2$) in which Coumarin 6 dissolves well and the TiO_2 particles do not sediment fast. When exposed to high pump intensities the BzOH solution degrades rather quickly, whereas the the $Pm(OH)_2$ sample is more stable.

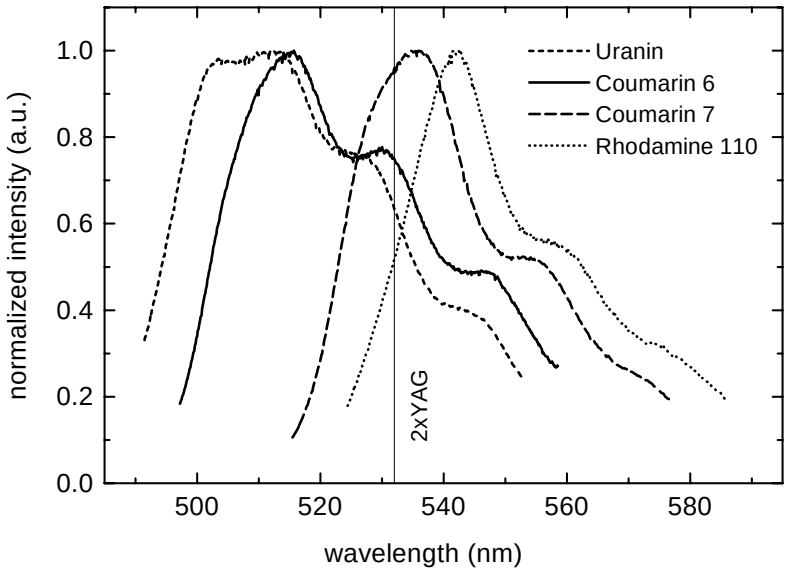

figure 2.4 *Fluorescence spectra of different green dyes dissolved in methanol. The dye molecules are excited by low energy tripled Nd:YAG (355 nm) pulses.*

red dyes
Since the probe beam we want to use for the red dyes is tunable, we do not have to make a spectral selection here. We can take a commonly used dye with a good emission efficiency. The dye should be pumpable with the second harmonic of a Nd:YAG (532 nm). We choose Sulforhodamine B (or Kiton Red), of which we measured the emission spectrum shown in figure 2.6a. The dye is dissolved in methanol as indicated in [13].

2.3.2 spectral narrowing and peak shift

green dyes
When the scattering Coumarin 6/$Pm(OH)_2$ sample ($\ell = 10\ \mu$m, $\ell_i \approx 100\ \mu$m) is pumped by a laser beam of variable intensity, it shows a clear spectral narrowing (figure 2.5). The width of the pulsed spectra decreases from 34 nm at 0.4 mJ mm^{-2} excitation to 7.8 nm at 1.7 mJ mm^{-2} (at 2.5 mm diameter). A red shift is also observable. The peak position changes from 525 nm to 527.5 nm (here also the two spectra of pulsed excitation are compared).

red dyes
The Kiton Red samples also show a spectral narrowing (figure 2.6b), from 34 nm at 2.0 μJ mm^{-2} excitation to 7.0 nm at 0.4 mJ mm^{-2} (at 1.2 mm diameter). In this measurement no significant peak shift seems to occur.

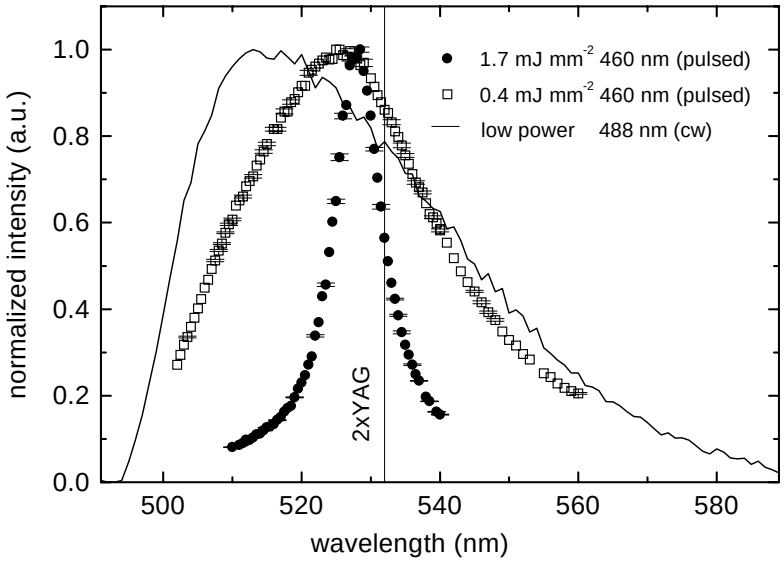

figure 2.5 *Fluorescence spectra of Coumarin 6 in 2-methyl-2,4-pentanediol and TiO_2-particles. A spectral narrowing is clearly visible when the pump energy is increased. The spectra of the two pulsed excitations are red shifted by 2.5 nm with respect to each other.*

2.3.3 determining the threshold

In order to measure the threshold of our system, we monitor the fluorescence through a monochromator as a function of pump energy. The monochromating spectrograph is set at the peak wavelength of the narrowed spectrum.

green dyes
For the Coumarin 6 solution the spectrograph is set at 527 nm with a window of 1 nm. Going from low to high pump energy we observe (figure 2.7) an upwardly curved behaviour up to 0.5 mJ mm^{-2}, then a linear part between 0.5 and 1.8 mJ mm^{-2} and finally at higher pump energies a deviation from this linearity. The left part of the figure shows a threshold, as it was described in section 2.1. When extrapolating the linear part we find the threshold of our system at the intersection with the horizontal axis, at 0.22 mJ mm^{-2}. The breakdown of the linear dependence at pump energies higher than 1.8 mJ mm^{-2} is caused by the 'burning' of the TiO_2-particles.

Exposure to a high-energy laser beam causes the TiO_2 to turn black, even when we repeated this with uncoated particles where the beam is incident on a quantity of plain powder without solvent, dye, or contact with glass.

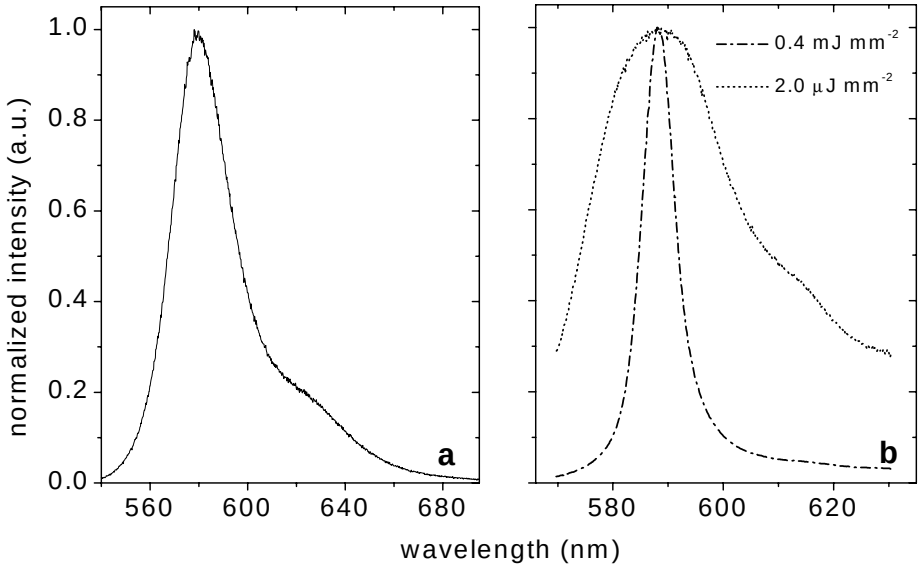

figure 2.6 *a) Fluorescence spectrum of Kiton Red dissolved in methanol. The dye molecules are excited by low energy doubled Nd:YAG (532 nm) pulses. b) Spectra of Kiton Red in methanol with TiO_2 scatterers. Two pumping intensities are used to show the spectral narrowing.*

red dyes

The spectral window is set at 589 nm. The width of this window is 1 nm. As can be seen from figure 2.8 the same behaviour as in the Coumarin 6 case is found. The threshold for the Kiton Red sample is determined to be 19 μJ mm^{-2}.

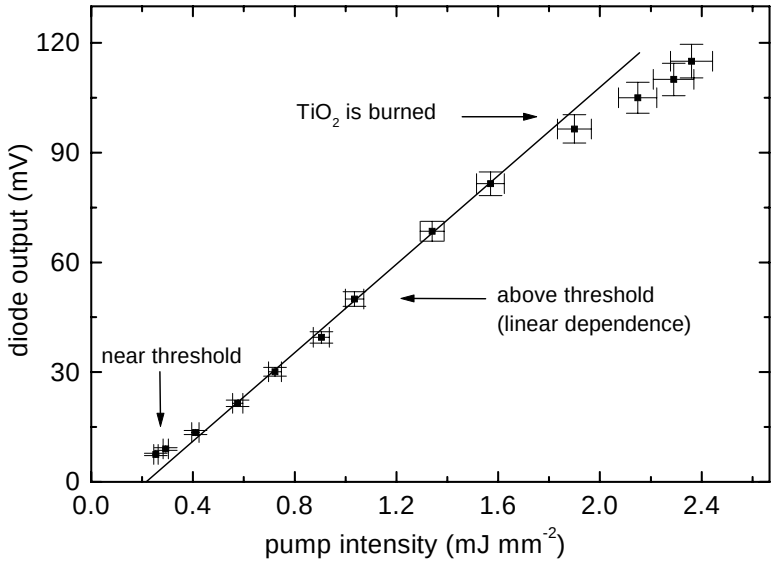

figure 2.7 *Input-output characteristic for Coumarin 6 in 2-methyl-2,4-pentanediol with TiO_2-scatterers. The outcoming light is monitored at 527 nm in a window of about 1 nm. A threshold shows up at 0.22 mJ mm^{-2} above which the output intensity shows a linear dependence. At very high pump intensities the linear dependence breaks down because the TiO_2-particles become black.*

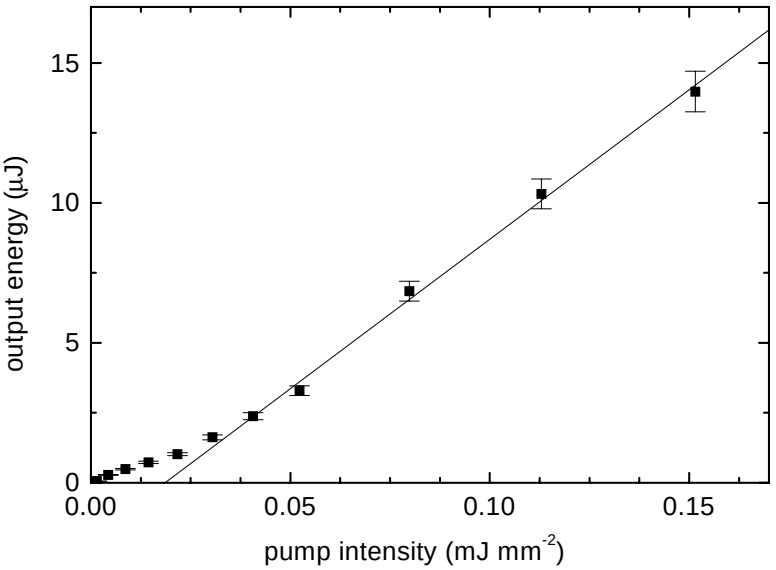

figure 2.8 *Input-output characteristic for Kiton Red in methanol with TiO_2-scatterers. The outcoming light is monitored at 589 nm in a window of about 1 nm. A threshold shows up at 19 μJ mm^{-2} above which the output intensity shows a linear dependence.*

2.4 conclusions

We have chosen our samples for our further experiments and have observed their spectral narrowing effects. We have determined the laser threshold (by extrapolation from the high pump intensity regime) for our Coumarin 6 in 2-methyl-2,4,-pentanediol samples to be around 0.22 mJ mm^{-2} for a 2.5 mm diameter pump beam. This we cannot at the moment compare with literature, since random laser experiments using this dye-solvent combination have not been performed so far.

The threshold of the Kiton Red suspension is determined to be 19 μJ mm^{-2} for a 1.2 mm diameter pump. This is about half the value found in [15], but there a ℓ of 100 μm was used, instead of 10 μm. It is known from a.o. [21] that the introduction of scatterers tends to lower the threshold intensity.

When we compare the threshold intensities of the Coumarin 6 suspension and the Kiton Red suspension, it is seen that the first one is about ten times higher than the second one. This could be due to the difference in laser efficiencies which are respectively $< 9\%$ for Coumarin 6 and 20% for Kiton Red [13]. A higher efficiency means a higher emission rate and therefore there will be more stimulated emission which causes the spectrum to narrow.

3 speckle statistics

An interesting feature of random laser to look into are the statistical properties of the emitted light. In an ordinary laser, as we saw in chapter 1, the number of photons per mode gets a different distribution when the threshold is exceeded. For a random laser is is interesting to investigate if the number of photons per specklespot will also be subject to threshold crossing. But one can also think of intensity correlation measurements (input-output intensity) with respect to time, spatial correlations with respect to pumping intensity, or intensity correlations with respect to the probing angle. In our experimental work we have looked at two of these subjects: the intensity distribution of speckle and their spatial correlation (i.e. their average diameter) as a function of pumping energy.

3.1 distribution of speckle intensities

When ordinary laser light is scattered from a rough surface all its phase and directional relations are scrambled in a random way. Now, when for example a screen or wall is placed in the vicinity of the scattering surface, a characteristic pattern of high and low intensities becomes visible (figure 3.1). This pattern is called speckle and is caused by the constructive and destructive interference of the scattered light. We can now say something qualitative about the intensity probabilities of a speckle pattern. Scattering and interference of light are phenomena involving the amplitude and the phase of the electric field. For a monochromatic wave the analytic form of the electric field is

$$u(x, y, z; t) = A(x, y, z; t)\ \mathrm{e}^{i\omega t} \tag{3.1}$$

where $A(x, y, z)$ is the complex amplitude. The time dependence of the field is expressed by the exponential term. The complex amplitude A is composed of contributions

$$a_k(x, y, z) = |a_k(x, y, z)|\ \mathrm{e}^{i\phi_k} \tag{3.2}$$

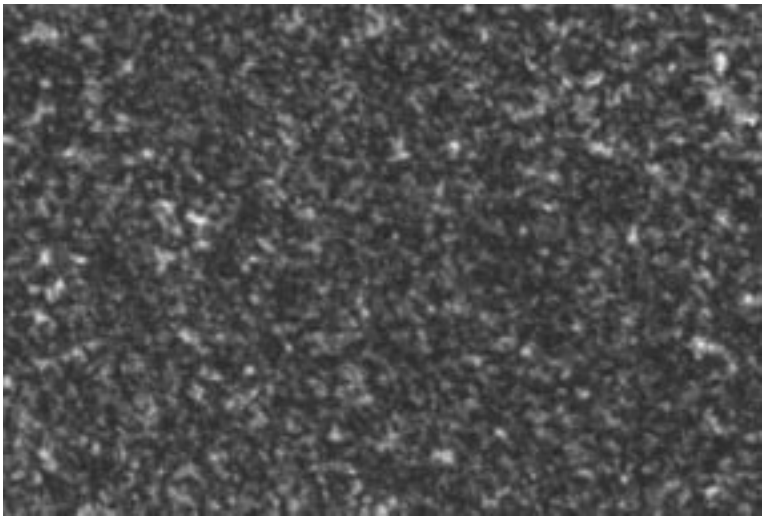

figure 3.1 *Speckle pattern of a doubled Nd:YAG using a piece of white paper as a scattering surface.*

called phasors, from every single point of the rough surface. This is to say that from different points on the rough surface we receive contributions with different field amplitudes $|a_k|$ and different phases ϕ_k. The total amount of electric field at the observer is the sum of these contributions

$$A(x,y,z) = \frac{1}{\sqrt{N}} \sum_{k=1}^{N} |a_k(x,y,z)| \ \mathrm{e}^{i\phi_k(x,y,z)} \tag{3.3}$$

where $\frac{1}{N}$ is inserted as a proper normalization on A. We can work out this sum statistically if we assume that

(i) the amplitudes $|a_k|$ and the phases ϕ_k for every k-value are statistically independent of each other and of all other phasors. This is to say that the elementary scattering areas of the rough surface are independent and that the strength of a given component bears no relation to its phase.

(ii) the phases ϕ_k are uniformly distributed on the interval $[-\pi, \pi]$, which expresses that the surface is rough on a wavelength scale.

Now we can compare the addition of the phasors with making a random walk in the complex plane. For $N \to \infty$ this leads to a Gaussian probability function for the field amplitude [22]

$$P(|A|) = \frac{1}{\langle |A|^2 \rangle} \ \mathrm{e}^{-|A|^2/\langle |A|^2 \rangle} \tag{3.4}$$

What we observe, however, are intensities, so we have to rewrite this relation

into an intensity distribution, using $I = |A|^2$

$$P(I) = \frac{1}{\langle I \rangle} \, \mathrm{e}^{-I/\langle I \rangle} \tag{3.5}$$

which is a simple exponential relation. We can see from this that if the incident intensity is increased, the amplitude at $I = 0$ goes down, and the distribution gets broader. For our experiments it is important that we can get the intensity out of the slope of a graph of the probability distribution. The calculation above holds for a scattering surface, suspended scatterers in a solvent and our random lasing samples when they are well below threshold. What will happen above threshold is subject of our investigations. The presence of stimulated emission might break down the condition (ii) concerning the independence of the scattering areas.

3.2 spatial correlations

Instead of throwing away all spatial information of a speckle picture by decomposing it and counting intensities only, we can also look at influences on the dimensions of the speckles. The correlation length of the intensity pattern can be called the average size of a speckle spot. This speckle size is connected with the roughness scale of the scattering surface compared to the wavelength of the scattered light and the dimensions of the illuminated surface [22]. The smaller the irregularities of the surface, the smaller the speckle spots. A smaller wavelength also yields smaller speckles and a smaller illuminated surface will result in larger speckles. All of these effects are comparable to what one can observe with an ordinary grating. The line density on the grating determines the spreading of the maxima. This is again relative to the wavelength of the light used. Furthermore, when a larger part of the grating is illuminated, the maxima get narrower.

For the random laser case the spatial correlation of its speckle pattern could be an interesting property to monitor while the amount of inversion in the system is changed. Well below threshold it should behave just like an ordinary diffuse scattering system, but when a reasonable amount of amplification is present, this might be observable in the speckle pattern. A lot of relevant system parameters could be subject to changes:

Above threshold the speckles are for a large part built up from stimulated emission, which might alter the form of the intensity probability distribution (as suggested at the end of section 3.1), and this will then probably have its effects on the spotsize: if the positions of constructive interference in the speckle pattern are fixed, then a change in the distribution of the high and low intensities must involve a change of the spotsize.

Secondly we expect a decreasing influence of higher gain on the spot size due to a geometrical cause. When the pumping intensity is increased, pump light is spreading over a larger volume and so the inversion volume becomes larger. The probe light will be amplified in a larger volume and the effective surface from which the light emerges is expanding (figure 3.2). We can consider this as an increase in the number of random light sources taking part in the interference that constitutes the speckle pattern. This has the same effect as a larger illuminated area on a passive scattering surface: the average speckle spot size will decrease. Since the crossing of the threshold will not be expressed in the size of the inversion volume, a decrease of the speckle spot size due to larger source dimensions can be expected to have no relation to the threshold intensity.

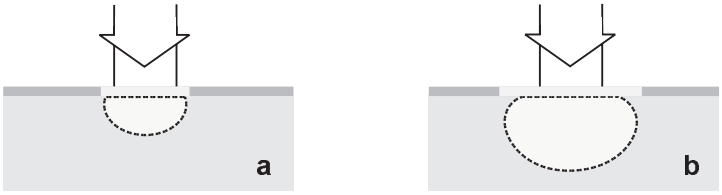

figure 3.2 *Form of the inversion profile. a) at low pumping energy, b) at higher pumping energy. The dimensions of the gain volume become larger when the pumping energy is increased. Probe light will be amplified in a larger volume and the effective surface from which the light emerges is expanding. From outside the medium this is observable as an increase of the source dimensions, which is indicated by the light-coloured part of the surface.*

3.3 experiment

For the experiments on intensity statistics and spatial correlations we use the setup in figure 3.3. Two laser beams coming from a Coherent Infinity laser are incident on our random lasing material. One beam is a frequency doubled Q-switched Nd:YAG at a wavelength of 532 nm and the other is a tunable beam from an XPO parametric resonator, pumped with the third harmonic of the Nd:YAG. Both of them are operated at a frequency of 10 Hz and at maximum energy (600mJ) of the fundamental frequency of the Nd:YAG in order to get the most stable output of the system. The beams are independently variable in energy by a system of Glan-prisms (which are not shown in figure 3.3). A Glan prism is a polarizing beam-splitter and two of them can be used to vary the intensity of a high-energy laser beam. The first prism is turned around

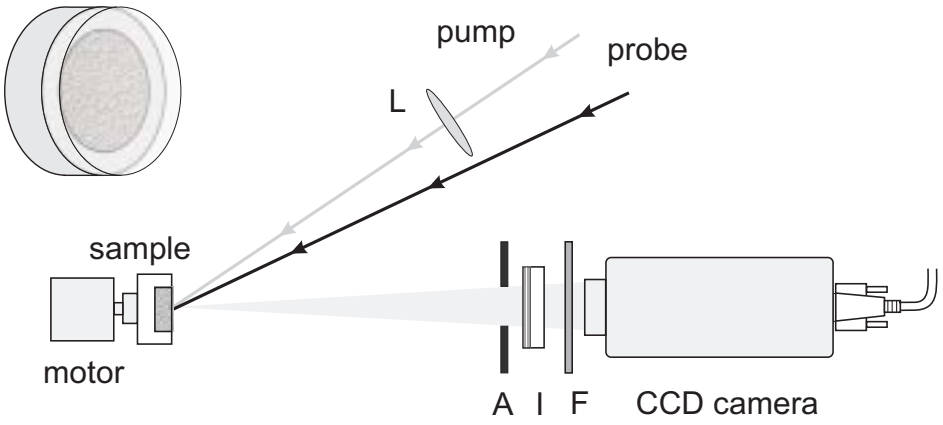

figure 3.3 *Setup for speckle statistics measurements. A pump and a probe beam are incident on the sample, which is mounted on a slowly spinning motor to prevent bleacing of the dye and sedimenting of the scatterers. Since the radius of the pumping beam is rather large a lens (L) is inserted. The light coming from the sample passes an aperture (A), an interference filter (I), and one or more neutral density filters (F). The image is recorded with a CCD camera operated by a pc. In the upper left corner the sample container is depicted in greater detail. On the front side a thick glass window is placed to diminish the influence of reflections.*

the beam axis to reflect an amount of light out of the beam. The second prism is kept fixed and determines the polarization direction of the ongoing beam. For these measurements the XPO beam is tuned to 480 nm, serving as a pump for the Coumarin 6 dye that we use for this experimental part. The frequency doubled YAG at 532 nm is used as probe. The high longitudinal coherence of this beam ($\approx$ 15 cm) is a condition for the observation of speckle. The dye and scatterers concentration are the same as the Coumarin 6 samples in the previous chapter, with $\ell \approx 10$ μm and $L_a \approx 100$ μm. The sample is put in a holder with a thick front window, in order to diminish the effect of multiple reflections (inset of figure 3.3). The holder is mounted on a motor turning at low speed to prevent the TiO_2-scatterers from sedimenting and the dye from bleaching. The pulses of the two laser beams are synchronized at the position of the sample by leading one of the beams over a delay line (not shown in the figure). The speckle pattern is recorded one shot each picture with a CCD camera (768 by 512 pixels).. Before the light enters the camera it is monochromated by an interference filter at 532 nm.

3.3.1 intensity statistics

We have looked at intensity statistics both as a function of pump intensity and as a function of probe energy. Measurements with variable probe intensity are included to investigate whether the amount of probe light can influence the relative contribution of spontaneous and stimulated emission (an extreme case of this changed ratio is injection locking [5]). When we put the pixel values of a CCD image of speckle in a histogram the result typically looks like figure 3.4a (plotted logarithmically).

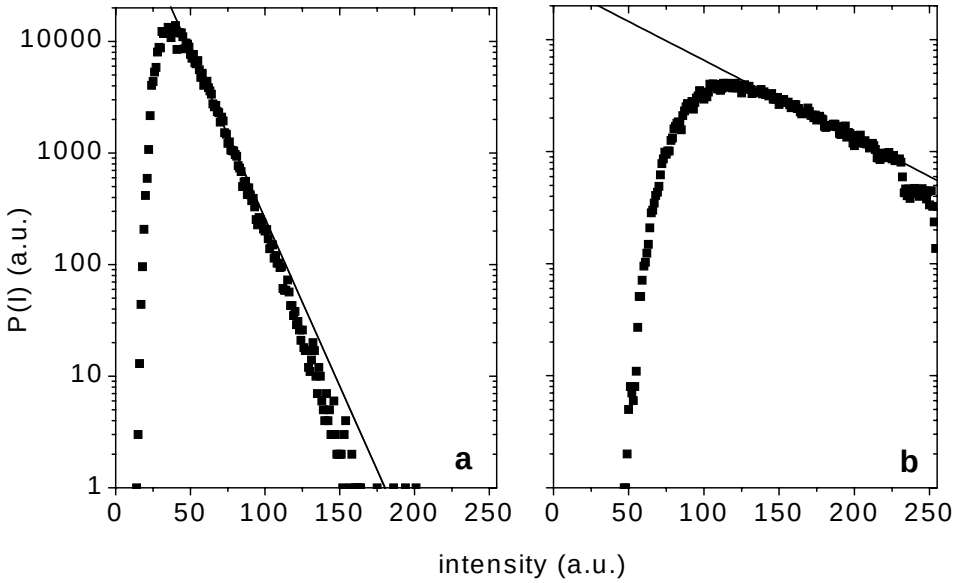

figure 3.4 *Typical intensity histograms of our statistics measurement. a) is a histogram at low pumping energy (0.04 mJ mm^{-2}) and b) at high energy (1.7 mJ mm^{-2}). On the x-axis there is the pixel value of the CCD camera, ranging from 0 to 255, which is proportional to the real intensity of the speckle pattern. A negative exponential behaviour is present at higher pixel values. The low probability of lower intensities is due to spontaneously emitted light, which is incoherent and therefore causes a diffuse background of which every pixel detects some light.*

One can see that the curve shows an exponential behaviour as predicted in section 3.1, but only for the higher intensities (high pixel values). At lower intensities we notice a diffuse background of spontaneously emitted fluorescence light. This light is incoherent and does not show speckle. Therefore the value of every pixel is increased with this background value. Figure 3.4b shows a histogram at a higher pumping intensity. The slopes of different histograms are fitted with an exponential, from the point onward where the influence of the fluorescence background is negligible.

In figure 3.5a we have put the inverse value of the slopes of the histograms (which is proportional to $\langle I \rangle$, section 3.1) in a plot as a function of pump energy.

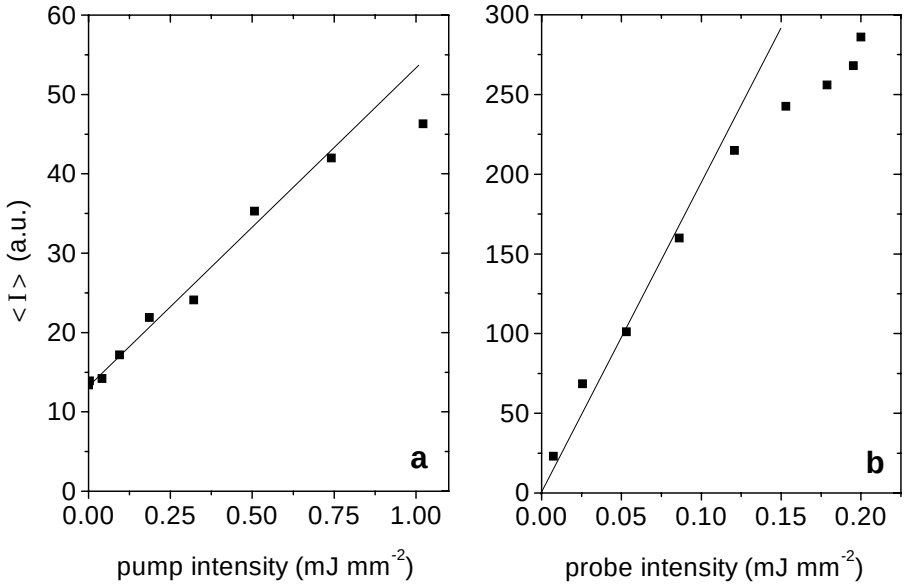

figure 3.5 *a) mean speckle intensities as a function of pump energy and a fixed low probing intensity (59 μJ mm^{-2}). From the measured data points a linear dependence can be supposed. The threshold of 0.22 mJ mm^{-2} as found in the previous chapter does not show up. b) Mean speckle intensities as a function of probe energy with a high pumping intensity (2.9 mJ mm^{-2}). The dependence on probe intensity is linear.*

We can see that there is a trend of increasing $\langle I \rangle$ when the pumping energy is increased, which indicates that probe light is amplified by the medium (at higher pumping intensities the fluorescent background also increases, but this is not measured here, since we take the intensities from slope of the histograms). Just as we do not see any effects of the crossing of the threshold in the form of the intensity histograms, we also do not see any effects from the measurements of $\langle I \rangle$. The positive cut-off of the y axis is a measure for the probe intensity.

The same intensity measurements have been done with a fixed high pump energy of 2.9 mJ mm^{-2}, well above threshold for these samples, and a variable probe beam (figure 3.5b). What we see is again a linear dependence of the mean intensity on the probe intensity. The straight line intersects the origin, as it should, because no coherent source is present. At higher probe intensities the experimental data show a deviation from the straight line, which is probably

due to overexposure of the CCD camera. All intensity histograms can be fitted well with an exponential decay.

3.3.2 spatial correlations

The measurements on the mean speckle diameter have been performed using the same two series as above: first as a function of pump energy with a low constant probe intensity, secondly as a function of probe energy with a high constant pumping intensity. The two-dimensional spatial correlations have been determined using the Fast Fourier Transform algorithm (FFT). By Fourier transforming, taking the absolute value squared and Fourier transforming back, we get the 2-D autocorrelate (inset in figure 3.6). This we fit with a negative exponential allowing for a possible directed axis (although we do not expect to find one).

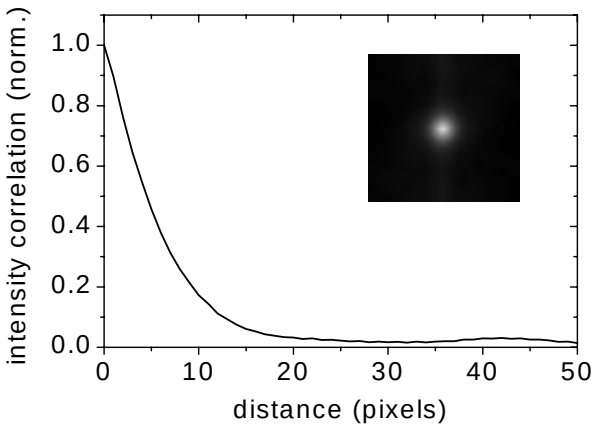

figure 3.6 *Example of a speckle correlation measurement for one specific value of the pump and probe intensities. The inset shows the 2-dimensional correlation and the graph is the circularly averaged value of this correlation. The width of this graph is a measure for the correlation length, or equivalently the average speckle size.*

The width, or decay distance, of this exponential (figure 3.6) gives a measure for the mean speckle diameter, which determines the correlation angle for light leaving the sample. We can now put the values we obtain from the first series in a plot against pump intensity (figure 3.7a) and the values of the second series against probe energy (figure 3.7b). The features of these plots are different. The first plot shows a clear decrease in of the angular correlation with increasing pump energy. The decay distance decreases rapidly from 6.1 pixels and saturates at about 4.3 pixels. The increase of the probe energy in the second plot does not seem to have any effect. We can explain this by invoking the mechanism we discussed in section 3.2. Since ℓ of the samples

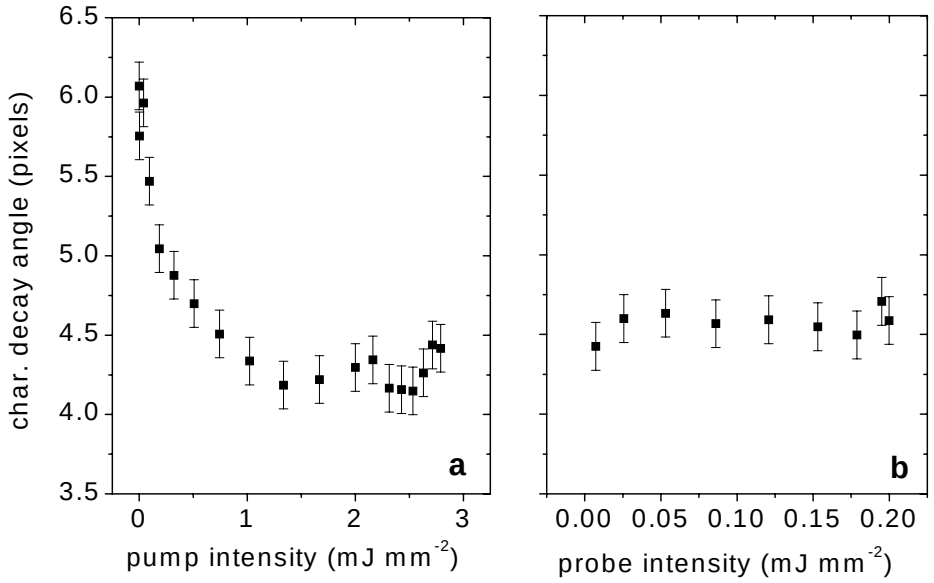

figure 3.7 *Mean speckle spot size, or angular correlation length. a) as a function of pumping intensity with a constant probe of 59 μJ mm^{-2}. The speckle size decreases with increasing pump intensity and seems to saturate at about 4 pixels. b) as a function of probe intensity with a fixed pump intensity of 2.9 mJ mm^{-2}. Increasing the probe power leaves the mean spot size unaffected.*

used here is 10 μm and L_a of the order of 100 μm, we expect to have a broad and flat gain profile. So when the pumping intensity is increased, the effect of increasing source dimensions will be important, and the angular speckle correlations get smaller. In the second plot, upon increasing the probe energy at constant pumping, the speckle spot size does not change. This is as expected because all paths become proportionally more intense[1].

[1] An influence of non-linearity due to injection locking effects could maybe disturb this, but in our measurements the possible effects seem to be negligible

3.4 conclusions

The distributions of speckle intensities do not seem to change shape when the 'lasing' threshold is crossed. All intensity histograms could be fitted well by exponential decay (for their higher pixel values). It could be that the possible effects are too subtle to show up in these experiments, for example they could be obscured by the background of fluorescent light which distorts the single exponential decay at lower intensities. It could also well be that there are no observable effects at all connected with the threshold crossing. When the average intensities $\langle I \rangle$ are extracted from the slopes of these histograms, it is found that the dependence on pumping intensity is linear. Although the fluorescent background value is be influenced by the crossing of the threshold (since this is exactly the input-output intensity measurement that was done in the previous chapter), there is no sharp transition in the amount of amplification of probe light. The dependence of $\langle I \rangle$ on probe intensity also shows a linear dependence. There are no indications of a changing spontaneous and stimulated emission ratio.

In our measurement on the speckle size with variable pump intensity also no threshold influence seems present. The decay angle decreases smoothly from 6.1 to 4.3 pixels and saturates at this last value. The suggested influence of changing intensity statistics on the speckle size (section 3.2) could not be demonstrated, since the statistical change itself could not be observed (see above). A decrease of the spot size can be explained satisfactorily with the spreading source mechanism discussed at the end of section 3.2. Since a decay distance of 4 pixels is well within the experimental resolution, a physical explanation for the saturation has to be sought. We have none available yet. Increasing the probe intensity does not have any influence on the speckle spot size, as is to be expected assuming that all lightpaths become proportionally more intense.

Much more statistical research on random lasers could and should be done than the experiments presented here. Particularly interesting are experiments on random lasers in a solid matrix. This configuration has the advantage over the liquid samples used here, that one selected speckle spot can be monitored during different shots of the laser system, allowing for other correlation measurements (in our experiments the speckle patterns are changing due to the motions of the scatterers). We have made an attempt to produce solid random lasing material: glass containing dye and TiO_2 particles, obtained through sol-gel synthesis. We did not succeed, however, due to the sedimenting of the scattering particles and the aggregation of the dye during the ageing of the gel.

4 enhanced backscattering

The most important part of our experiments is the recording of light that is scattered from random lasing samples in the backward direction. As early as in the sixteenth century it was reported by an artist named Benvenuto Cellini that, standing in a group of people, he observed a bright halo around the shadow of his head and not around the heads of the others [23]. He interpreted it not too modestly as a token of his genius. We now look upon this as one of the first records of enhanced backscattering, a phenomenon any person could see around the shadow of his or her own head if the right conditions are present.

4.1 introduction to enhanced backscattering

As we have pointed out in chapter 3, a laser beam incident on a random scattering medium produces a spatial speckle pattern of high and low intensities. If the scatterers in the sample are able to move, or if the sample itself is moving, the points in space where the light interferes constructively and destructively are changing position and the speckle pattern averages out if one observes it at a long enough timescale. There is however one interference effect that will survive: there will be an increased intensity in a small solid angle around the direction of pure backscattering. This effect is referred to in literature as enhanced backscattering, sometimes as weak localization, or less correctly as coherent backscattering. The first theoretical analysis of the effect is found in [24] concerning radar backscattering. Enhanced backscattering of light has been confirmed experimentally in the mid-eighties [25, 26, 27].

In short, enhanced backscattering is the result of interference of counter-propagating waves which is always constructive in the direction of the incident wave. Considering light going into the medium at a certain point A, then being multiply scattered and leaving the medium at some point B, we can see

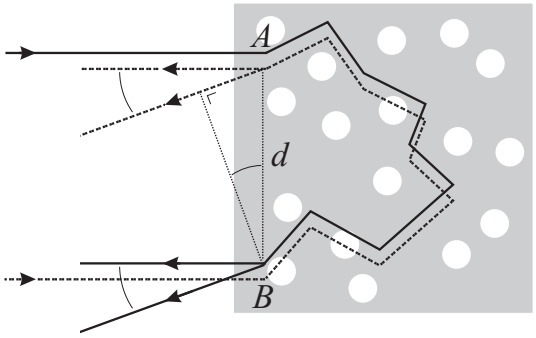

figure 4.1 *Schematic picture of enhanced backscattering. One light path is traveled in opposite directions and the outcoming waves interfere. For the exact backscattering direction this interference is constructive because the paths of the waves are equal and so are their phases. Light that comes out at an angle ϑ acquires a phase difference because of the difference in path length of $\Delta l = d \sin \vartheta$ and the resulting intensity is an oscillating function of ϑ.*

that a wave traveling along this path in the opposite direction, entering at B and leaving the sample at A, has exactly the same path length and thus the same phase upon leaving the sample (see figure 4.1). The two waves interfere constructively in the exact backscattering direction and their amplitudes add up. Assuming an equal amplitude for the counter-propagating waves ($A_1 = A_2 = A$) we can see that the resulting intensity is twice the intensity were there no interference:

$$\begin{aligned} I = (A_1 + A_2)^2 = A_1^2 + 2A_1A_2 + A_2^2 = 4A^2 \quad & \text{constr. interference} \\ I = A_1^2 + A_2^2 = 2A^2 \quad & \text{no interference} \end{aligned} \tag{4.1}$$

When we look slightly off-axis, a difference in path length is produced and the corresponding phase difference will make the interference less constructive. Again assuming equal amplitudes, the angular dependent intensity becomes

$$I(\vartheta) = I_0 \, (1 + \cos \frac{2\pi \; d \sin \vartheta}{\lambda}) \tag{4.2}$$

where d is the distance between the points where the light path enters the medium and the point where it leaves, λ the wavelength of the light and I_0 the intensity were there no interference effects. We see that the intensity is a goniometric function of the exit angle (figure 4.2, left).

Of course there is not one but many light paths and they all contribute to the backscattering intensity. Different paths will have different starting and ending points, which will yield different values for the distance between them, d. As can be seen from equation (4.2), these distances will determine the

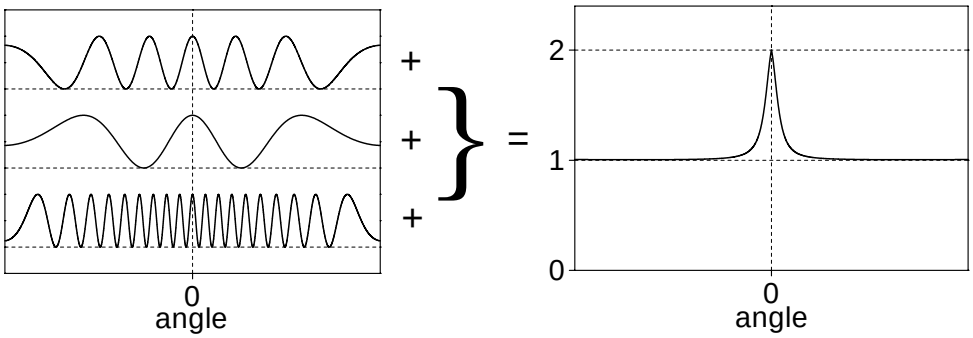

figure 4.2 *left: The interference patterns of light coming from the exit points of a light path and its counter-propagated path. Patterns are shown for three values of the distance between the exit points, d. right: When for a realistic system all interferences are added, the result is a characteristic peak, the enhanced backscattering cone.*

periodicity of the intensity profile. Large d will produce fast oscillations and small d slow ones. Although differing in period, all oscillating contributions have their maximum value for $\vartheta = 0$. If we sum many of them with different d, contributions around $\vartheta = 0$ add and the rest averages out. We find a characteristic peak, the so-called enhanced backscattering cone, that has a strong dependence on the exit angle (figure 4.2, right). In fact, if we would make the addition for any d, all contributions having the same weight, the result would be a δ-function.

That we do not observe a δ-function has several reasons. First, d cannot grow infinitely, because it is limited to the beam diameter. Furthermore—and this is the more interesting part, because from this we can infer properties of the system—the weights of contributions with different d are not equal. The value of the distance d between the starting and ending points of a light path is related to the total length of this light path s: long paths will on the average end up at a large distance from their starting point, short paths will leave the medium in the vicinity of their starting point. Therefore the probability distribution for the distance d is determined by the path length distribution $P(s)$ of light in the system. If, for example, short paths are favoured over long ones, slowly oscillating contributions with small d will be more important and the backscattering cone will be wide.

In an ordinary (non-absorbing and non-amplifying) multiple scattering medium $P(s)$ is indeed large for short paths and small for long paths. This can be understood if we consider the diffusive process as a three-dimensional random walk, where one of the half-spaces represents the sample. The probability to make long paths with a large transverse displacement is small because of the increasing probability to end up in the wrong half-space and thereby

having left the sample. Since in non-absorbing media contributions of path lengths up to infinity have to be summed, the peak of the backscatter cone is cusped, i.e. is not analytical at $\vartheta = 0$ [1].

The presence of absorption is an important factor reducing the probability of long paths. Absorption puts longer paths at a disadvantage because the intensity is proportional to e^{-l/L_a} (where l is the length of the light path). This will suppress the fast oscillating contributions to the backscatter cone very drastically, which will result in a rounded peak at $\vartheta = 0$. In our experiment, however, we realize amplification in the samples, so that longer paths will gain importance. Apart from this there are a number of other influences on the shape of the backscattering cone (like localization of light) which are beyond the scope of this thesis.

We have pointed out some factors determining the shape of the cone, but something more can be said about its height. Assuming that our incident laser beam has a flat transverse intensity profile we can say that the constructive interference at $\vartheta = 0$ of one pair of counter-propagating waves will result in an intensity that is exactly twice the intensity if there were no interference (equation (4.1)). However, this does not hold for the case that light is scattered back immediately by one single scatterer. Then there is no doubling of the intensity since the incoming and outgoing paths coincide and no interference takes place. We have to treat multiply and singly scattered light differently and separate the total backscattered light in a multiply scattered and a singly scattered component. So, the total backscattered intensity can be written as

$$I_{\mathrm{tot}}(\vartheta) = I_{\mathrm{d}} + I_{\mathrm{c}}(\vartheta) + I_{\mathrm{s}} \tag{4.3}$$

where I_{d} and $I_{\mathrm{c}}(\vartheta)$ represent the constant term and the angle dependent term from equation (4.2) respectively, both summed for appropriate values of d. The sum of I_{d} and I_{c} is the multiple scattering component of the backscattered light. I_{s} is the single scattering contribution. If we divide $I_{\mathrm{tot}}(0)$ by its value for large enough ϑ, for which the interferences of the multiple scattering component have averaged out and $I_{\mathrm{c}} = 0$ (we can call this value the background intensity), we find the enhancement factor of the backscattering cone.

$$E = \frac{I_{\mathrm{tot}}(\vartheta = 0)}{I_{\mathrm{tot}}(\vartheta \gg 0)} = \frac{I_{\mathrm{d}} + I_{\mathrm{c}}(0) + I_{\mathrm{s}}}{I_{\mathrm{d}} + I_{\mathrm{s}}} \tag{4.4}$$

[1] As was mentioned before, the finite beam diameter prevents d from becoming infinitely large, but when the diameter is large enough, the experimental resolution will not allow discrimination between a real, non-analytical, cusp and one which is only apparent.

In the discussion above, the components I_d and I_s were considered angle independent. Actually they do show a dependence on ϑ, which is due to the projection of the spherically symmetric emission of the source on a plane in which the emission is measured. This dependence usually does not show up in the limited angular region where the backscattering cone is measured and is therefore neglected.

Since $I_\mathrm{c}(0) = I_\mathrm{d}$, we can write for the enhancement factor

$$E = \frac{2I_\mathrm{d} + I_\mathrm{s}}{I_\mathrm{d} + I_\mathrm{s}} = \frac{2(I_\mathrm{d} + I_\mathrm{s}) - I_\mathrm{s}}{I_\mathrm{d} + I_\mathrm{s}} = 2 - \frac{I_\mathrm{s}}{I_\mathrm{d} + I_\mathrm{s}} \tag{4.5}$$

From this we can see that the enhanced backscattering cone has a height of twice the background intensity minus the single scattering component. For isotropic scatterers without absorption the single scattering contribution is about 12% [28], which yields an enhancement factor of 1.89.

It is possible to filter out singly scattered light by using a laser beam of circularly polarized light in combination with a quarter wavelength plate in front of the detector. For singly scattered light to be detected, it must scatter back exactly along its incoming path, thereby reversing its helicity. So, in the helicity conserving channel we do not detect singly scattered light, which results in an enhancement factor of 2, according to equation (4.5) with $I_\mathrm{s} = 0$. The enhancement factors considered here are the theoretical maximum values.

In order to observe enhanced backscattering it is not necessary to start with coherent light. This is the reason why we opted for the term enhanced backscattering and not for coherent backscattering. In fact any light source will do, provided that it has a small divergence and is transversely coherent. Sunlight therefore is suitable and this explains Cellini's observation. In experiments light of one specific wavelength is to be preferred: spectral broadness will blur the features of the backscattering cone. For these reasons in general lasers are used to record enhanced backscattering, but it is not inevitable. Actually it is favourable to have a low longitudinal coherence in order to diminish the inconvenience of speckle, which means the laser does not have to be very good.

To obtain a quantitative description of the cone shape, we make use of diffusion theory. When compared to cones calculated with rigourous scattering theory [28], there is a good agreement. Scattering theory predicts only slightly higher values for the wings of the cones. We will not pursue these matters here, but state the outcome and refer to literature instead [28, 29]. The normalized version of the interference contribution I_c, is generally referred to in literature

as the bistatic coefficient γ_c

$$\gamma_c(\vartheta_s) = \frac{3}{2\ell^3 \alpha u} \frac{\alpha + u(1 - e^{-2\alpha z_0})}{(u+\alpha)^2 + \eta^2} \tag{4.6}$$

where ϑ_s is the angle between the incoming wavevector $\vec{k}$ and the scattered wavevector $\vec{q}$. ℓ is the transport mean-free-path. $\alpha \equiv \sqrt{L_a^{-2} + q_\perp^2}$ in which L_a is the absorption mean-free-path, $q_\perp = k \sin\vartheta_s$ and $k = \frac{2\pi}{\lambda}$. $\eta \equiv k(1-\mu_s)$ with $\mu_s = \cos\vartheta_s$ (≈ 1 for small angles, which sets $\eta \approx 0$). $u \equiv \frac{1}{2}\kappa_e(1 + \mu_s^{-1})$ where κ_e represents the extinction coefficient given by $\kappa_e = \ell_s^{-1} + \ell_i^{-1}$ with scattering mean-free-path ℓ_s and inelastic mean free path ℓ_i. z_0 is the position of the so-called trapping plane, which is a correction needed in diffusion theory due to non-zero light flux on the sample boundary. It incorporates the internal reflection of the glass on the sample interface. The value of z_0 depends on the geometry of the sample and is of the order of 0.7ℓ. The expression for γ_c is valid, strictly speaking, only in the limit that the sample thickness L goes to infinity (semi-infinite slab), but will be a very good approximation provided that $L \gg \ell$.

The width (full width at half maximum, FWHM) W of the enhanced backscattering cone for non-absorbing and non-amplifying media and isotropic scatterers is expressed by

$$W = \frac{0.7}{k\ell} \tag{4.7}$$

in terms of the transport mean free path ℓ and the wavevector k (see [28]).

4.2 enhanced backscattering in an amplifying system

The expression of the cone in (4.6) is able to account for absorption in the system through the extinction and absorption mean-free-paths ℓ_i and L_a, but it is not trivial to incorporate amplification. One would expect the cone to narrow when there is amplification, since long paths are more amplified than short ones. As was argued above, this will increase the weight of contributions with larger d which make up the center of the cone. Attempts to adjust the theory for systems with amplification were done by inserting a uniform gain coefficient into the diffusion equation (see, for example [30], which also provides the first experimental data on the subject) that is the basis of the derivation of equation (4.6). This model is only valid for systems with a limited thickness L_{div}, above which the diffuse intensity diverges. When compared with experimental data it was found that the calculated cones showed too much narrowing, especially at high gain levels. This is not surprising since in realistic

configurations, because of scattering, light is amplified only in a confined part of the sample. Long paths move out of this region and get less amplification than one would expect on the basis of a uniform gain distribution. It follows that one has to put the gain profile explicitly into the calculations [31].

The enhancement factors of the backscattering cones can be expected to decrease with increasing pumping intensity. It is due to the increasing background of spontaneous, and at higher pumping intensities also stimulated, emission from the dye. This increase of the background is what we measured in chapter 2 as output intensity versus pumping intensity in a spectrally narrow interval. At higher pumping intensities, in the regime of the narrowing of the emission spectrum, the background intensity will increase more than proportionally with the pumping intensity.

To obtain the fits of the cones we present in this chapter, we use a numerical routine to calculate the gain profile (as described in [32], see figure 4.12 on the right), and the problem of finding the solution of the diffusion equation is transformed into solving the eigenvalue problem of a particle in a box (as in quantummechanics) with the gain profile subtracted from the bottom. This procedure is presented in [31].

4.3 experiment

In this experiment we have chosen to record enhanced backscattering by means of a fixed CCD camera instead of the more common method of scanning a certain angular range with a photodiode or photomultiplier tube. This makes our setup simpler, since the camera does not have to be aligned very accurately in the backscattering direction (we are able to find out afterwards where the peak of the cone is located exactly), and faster, because we are able to 'scan' a two-dimensional solid angle at once. A disadvantage is that our dynamic range is limited to the 8 bits of the camera and that our camera only allows to accumulate light in periods of 10 seconds.

The random lasing systems are the same as we used in the previous chapter: a dissolved laser dye (Coumarin 6 in 2-methyl-2,4-pentanediol and Kiton Red in methanol) in a suspension of TiO_2-particles with a diameter of about 220 nm. In order to measure enhanced backscattering of these samples we need two laser beams, one to induce inversion in the sample: the pump beam, and one of which the actual backscattering is recorded: the probe beam. The laser that we use here is a Coherent Infinity: a combined system of a frequency doubled Q-switched Nd:YAG (532 nm) and a tunable OPO system (400-700 nm) pumped by the third Nd:YAG harmonic. The laser produces pulses with a duration of 2 ns and 5 ns for the doubled Nd:YAG and the OPO respectively,

at a repetition rate ranging from single shot to 100 Hz. In order not to degrade our laser dye it is set at 20 Hz. The maximum pulse energies of the beams are 100 mJ for the Nd:YAG and 30 mJ for the OPO. The laser is operated at maximum output energy since this provides the best pulse height stability.

The intensities of the beams can be varied by a system of two Glan prisms for the OPO beam and two Glan prisms and a half wave plate for the doubled Nd:YAG. The beam that is used as a pump (we changed this during the experiment when we changed the dye and solvent) is led over a delay-line which is a movable prism, making the path of the light longer or shorter by twice its displacement[2]. The delay-line is set as to make the two pulses arrive at the same time at the sample. In figure 4.3 we depict the setup, where we have left out the laser itself, the attenuating systems for the pump and probe beams and the delay-line for the pump beam, in order to concentrate on the central parts. On the left we see the sample mounted on a spinning motor to average speckle, but also to prevent the dye from bleaching and the scatterers from sedimenting. The probe beam is incident on the sample via a beam splitter which is wedge-shaped so that the rear-side reflection does not reach the sample. The part of the probe beam which is transmitted through the beam splitter must be dumped very carefully because if it reaches some (only slightly) reflecting object, the light will enter the camera exactly at the point where the backscattering cone is. Therefore the ongoing beam is incident on a black glass plate mounted at the Brewster angle. In this way we will have lost already the largest part of the light. The remaining light will be reflected from the glass plate onto a piece of black velvet.

The light that is backscattered from the sample and transmitted through the beam splitter reaches the recording end of the setup. It passes, in this order, an aperture to reduce stray light, an interference filter to block scattered pump light, a lens, a polarization filter that transmits s-polarized light (which is parallel to the initial beam), and finally one or more neutral density filters, before it falls on the chip of a CCD camera (Kappa CF 8/1 FMC). The chip is in the focus of the lens (f = 75 mm, d = 60 mm) in order to make light from each different exit angle converge on a different point on the chip. The camera is connected to an exposure controller and to a frame grabber in a pc, producing grayscale bitmaps of 768 by 512 pixels. The configuration of lens and camera yields a resolution of 0.107 mrad per pixel, which is well within the beam divergence for the laser, being about 1.5 mrad.

The picture shows also the pump beam, which is focused by a lens (f = 25 cm). The focal point lies in front of the sample and by varying the distance from lens to sample, we can vary the size of the pumped region on the sample.

[2]It is the pump beam that is led over the delay-line, because the alignment of the probe beam is much more delicate and it might be disturbed by moving the prism, if the alignment of the delay-line were not perfect.

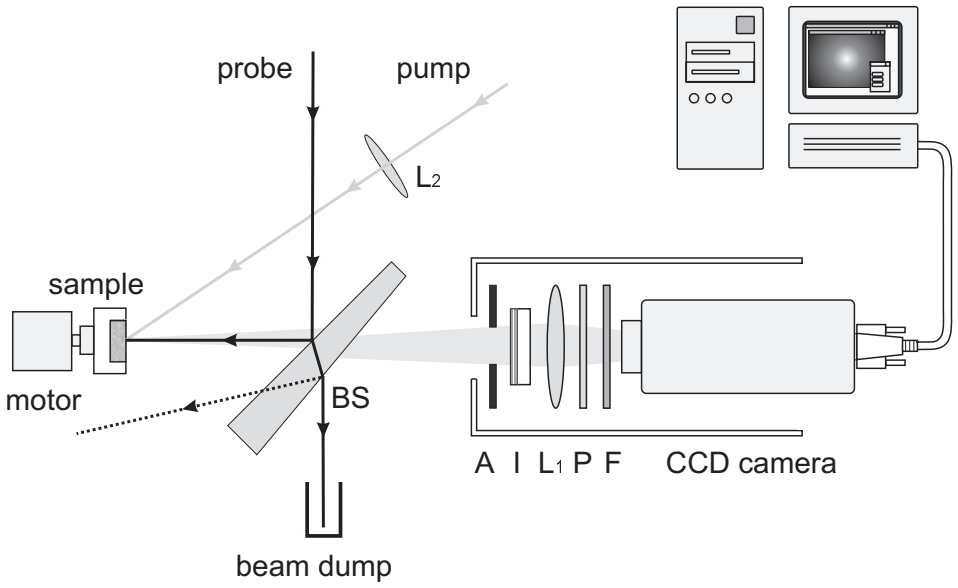

figure 4.3 *Setup for the recording of enhanced backscattering cones. The intensities of the pump and probe beams are variable by a system of two Glan prisms (for the XPO-beam) and two Glan prisms with a half wave plate in between (for the doubled Nd:YAG-beam). These attenuating systems are not shown in the picture. The probe beam is incident on the sample via beam splitter BS, which is slightly wedge-shaped to prevent the rear-side reflection from falling on the sample. Behind the beam splitter in the transmitted direction is a beam dump consisting of a black glass-plate mounted at the Brewster angle, reflecting the beam onto a piece of black velvet. To the right of the beam splitter, catching the backscattering direction from the sample, is a CCD-camera which is coupled to a frame grabber in a personal computer. In front of the ccd are: an aperture (A), an interference filter (I), a lens with a focal length of 75 mm (L_1) having the camera in its focus, a polarizer (P) letting through s-polarized light (which is the same as the initial beam) and one or more neutral density filters (F). The pump beam is focused by a lens with a focal length of 25 cm (L_2), which is placed such that its focus lies in front of the sample. The sample is mounted on a motor in order to average speckle and to prevent the dye from bleaching and the scattering TiO_2 particles from sedimenting.*

4.3.1 analysis of recorded backscattering cones

The bitmaps of enhanced backscattering cones consist of multiple shots of the laser. When we would have only one shot per picture, the speckle would not average, because on the timescale of the pulses (a few ns) the sample is essentially static. With the laser operating at 20 Hz and the acquiring time of the camera being at most 10.24 s, we have a maximum of 204 shots per bitmap (sometimes even less because we have to reduce the exposure time to

prevent overexposure). These 204 shots are still not enough to get rid of all speckle (see figure 4.4, left), so we can not just take an x- or y-section through the picture, for the cones will have too much noise. Instead, we determine the center of the picture and then fold it out around this point, transforming to polar coordinates. The φ-coordinate is summed to get a circularly averaged backscattering cone which is mirrored for aesthetic reasons (figure 4.4, right).

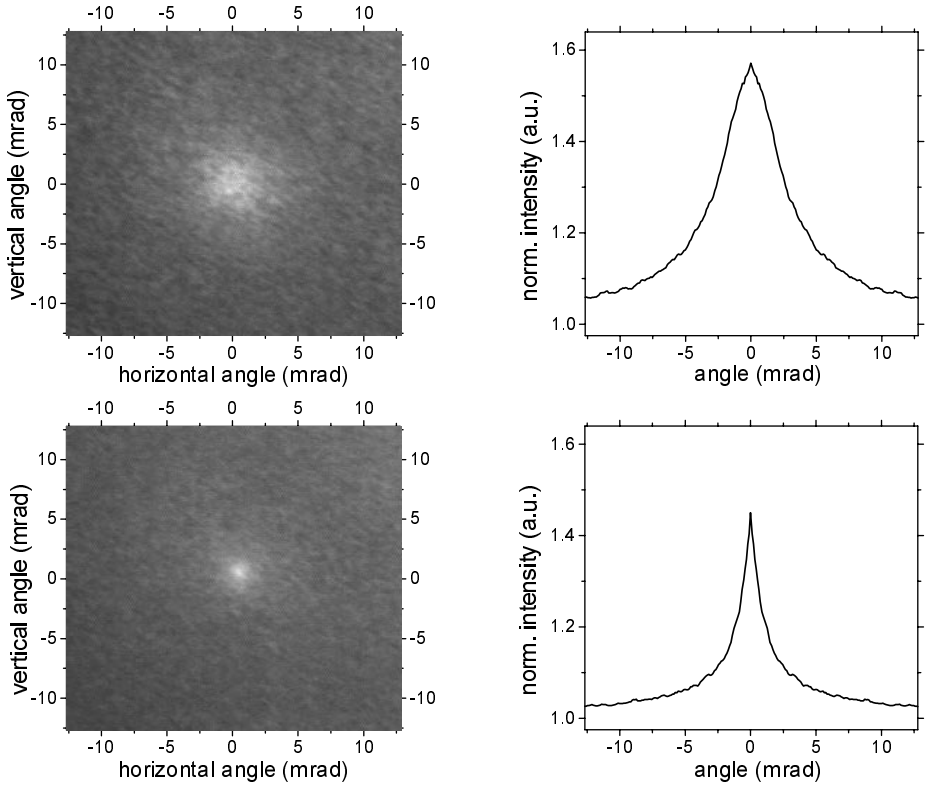

figure 4.4 *Examples of CCD images of enhanced backscattering cones of the Kiton Red samples with $\ell = 10$ μm (on the left, above without pump, below with pump of 78 μJ mm^{-2}) and the results after averaging concentric circles (on the right; the resulting radial profiles are mirrored). The 204 shots of which the CCD images are composed, are still not enough to average out all speckle, as can be seen most clearly in the image in the upper left corner.*

The determining of the center point is done by hand which proved a reliable method: a series of subsequent tries always produced the same result within one or two pixels. The rest of the procedure is done by computer. It must be noted that the values of the data point at zero angle (the top of the cone) and its neighbouring points are not very reliable, since the number of circularly averaged points is one in the center and increases quadratically with increasing ϑ.

4.3.2 random lasers with Coumarin 6 as gain medium

In contrast with the experiments of chapter 3, speckle is an unwanted phenomenon when recording enhanced backscattering cones. The higher the coherence of the probing beam, the more averaging has to be carried out in order to obtain reasonable quality cones. Since the averaging capacity of the CCD camera is limited (204 shots) it is sensible to use the OPO (coherence length $\approx$ 1 mm) as a probe rather than the Nd:YAG (coherence length $\approx$ 15 cm). This makes Coumarin 6 (which has to be pumped by the OPO, since it only absorbs in the blue) less suitable for backscattering experiments. We have actually measured a number of cones, but they do not seem to show any narrowing, for which we have no explanation. Added to this is the occurence of interference patterns due to the detection optics. No further experiments are performed on Coumarin 6 samples.

4.3.3 random lasers with Kiton Red as gain medium

We measured enhanced backscattering cones of Kiton Red in two systems with $\ell = 10$ μm and $\ell = 3$ μm as a function of pumping intensity. The probe frequency is set to 595 nm.

Kiton Red with $\ell = 10$ μm

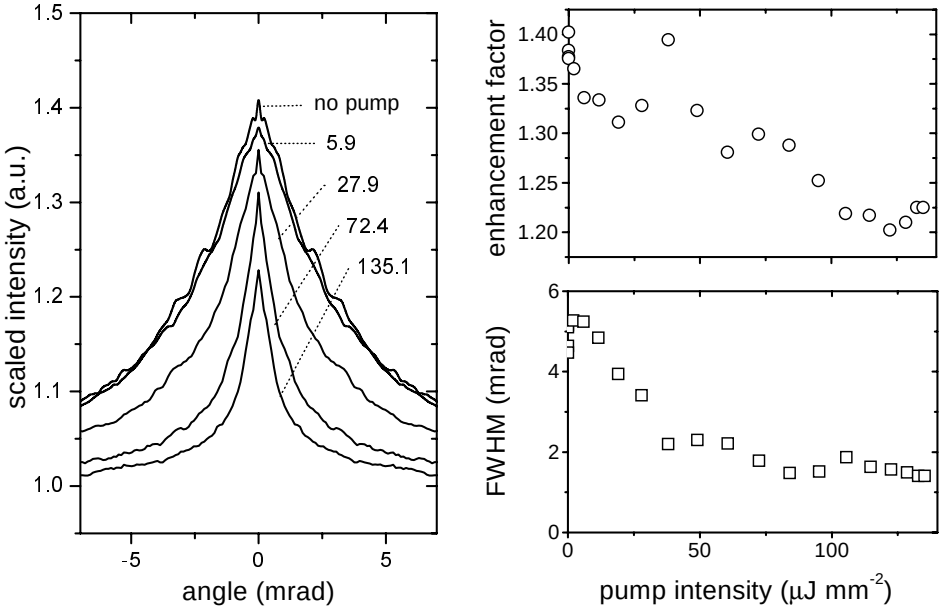

figure 4.5 *Enhanced backscattering cones of Kiton Red with $\ell = 10$ μm. In the left graph the pumping intensities (in μJ mm^{-2}) are indicated. In the right graphs the enhancement factor and the widths of the cones are shown.*

The decrease of the enhancement factor (figure 4.5 top right) can be explained by the increasing background of (amplified) spontaneous emission from the dye (section 4.2). When comparing the enhancement factor of the cone without pump ($E = 1.41$) to the theoretically predicted value ($E = 1.89$), we find a difference that is probably due to the presence of stray light, which will add to the background intensity.

As can be seen from the bottom right graph of figure 4.5, the widths of the backscattering cones decrease upon increasing the pumping intensity. This effect was predicted in section 4.2: more gain will favour long path lengths, which will increase the weight of contributions with a small angular dependence constituting the top of the cone.

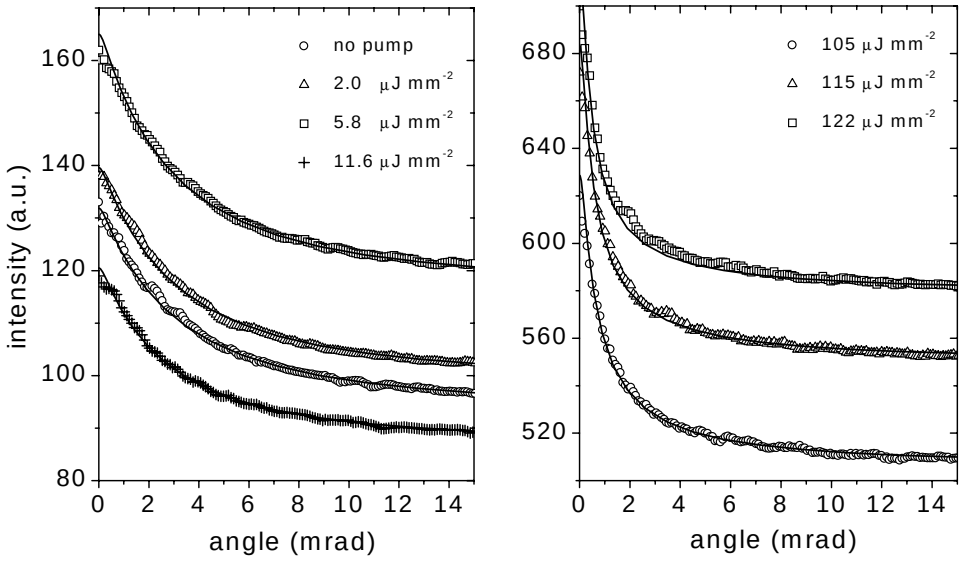

figure 4.6 *Backscattering cones (Kiton Red, $\ell = 10\ \mu m$) of low pump intensity (left) and of high pump intensity (right) fitted with scaled and off-setted theoretical cones from diffusion theory (solid lines). In both intensity regimes the fits can be made very good, which means that the experimentally found coneshapes for our amplifying system do not differ from shapes that are found by diffusion only.*

When the experimental cone shapes are compared to the theory of backscattering for a homogeneous gain profile (from [30]), it is found that they show too much narrowing when realistic values for ℓ and ℓ_g are used. However, the cones can be fitted accurately with unrealistic values (ℓ_g twice as large), which does not make this theory useful. The cones can also be fitted well with scaled and off-set theoretical cones incorporating only diffusion and no gain. This is done in figure 4.6, not in order to to extract quantitative information from the

data, but to expose differences in the shape between the backscattering cones with $\ell = 10$ μm and $\ell = 3$ μm. If the shape of the cone remains constant and only the width is scaled, this means that the transport mean free path ℓ can be replaced by an effective transport mean free path ℓ_{eff}, as adopted in the case of absorption [33], where

$$\frac{1}{\ell_{\text{eff}}} = \frac{1}{\ell_{\text{s}}} + \frac{1}{\ell_{\text{i}}} \tag{4.8}$$

In the case of gain we could substitute ℓ_{i} by $-\ell_{\text{g}}$ and we get

$$\frac{1}{\ell_{\text{eff}}} = \frac{1}{\ell_{\text{s}}} - \frac{1}{\ell_{\text{g}}} \tag{4.9}$$

To quantify the cone shape two parameters are used: the full width at half maximum (FWHM) and the top angle Θ. The top angle is found by extrapolating the slope of the cone near top to zero angle after subtraction of the background and normalization to 1 (see figure 4.7). The extrapolation has to be made because of the unreliability of the first few data points (section 4.3.1). Top angles from diffusion theory and experiment are compared in figure 4.8. If cones are to be described with a scaled ℓ_{eff}, then the tangents of the top angles can be fitted with a straight line through the origin. This can be done for both theoretical and experimental cones with $\ell = 10$ μm.

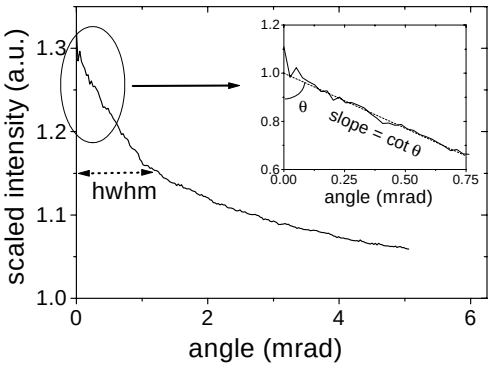

figure 4.7 *Procedure for extracting the width and the peak angle of the enhanced backscattering cones. In the inset the cone is shown after subtraction of its background ($\gamma_{\text{s}} + \gamma_{\text{d}}$) and normalization to 1. For small angles an extrapolation is made to zero angle, since the first few datapoints are unreliable due to our bitmap processing method. The angle between the extrapolated line and the y axis is assigned to be the top angle Θ.*

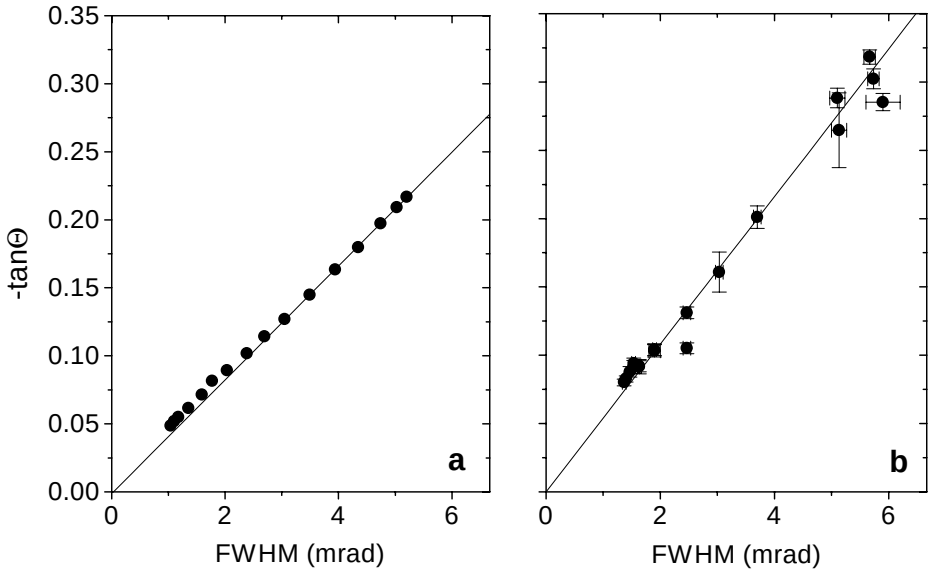

figure 4.8 *The tangent of the top angle* Θ *as a function of the width of the cone* ($\ell = 10\ \mu m$). *a) For cones from diffusion theory (with inhomogeneous gain). b) for the experimental cones. Both theoretical cones and experimental cones can be fitted by a straight line through the origin, which means they can be described by scaled diffusive cones with an effective transport mean free path.*

Kiton Red with $\ell = 3$ μm

Figure 4.9 shows the features of the backscattering cones for Kiton Red samples with $\ell = 3$ μm as a function of pumping intensity. The widths of the cones are roughly 4 times as large as those for the $\ell = 10$ μm samples. Here also the enhancement factors as well as the widths decrease with increasing pumping intensity. The enhancement factors are higher than those of the $\ell = 10$ μm samples. This can be due to improved stray light screening, but also to a more careful analysis of the cones using a fitted background $\gamma_s + \gamma_d$.

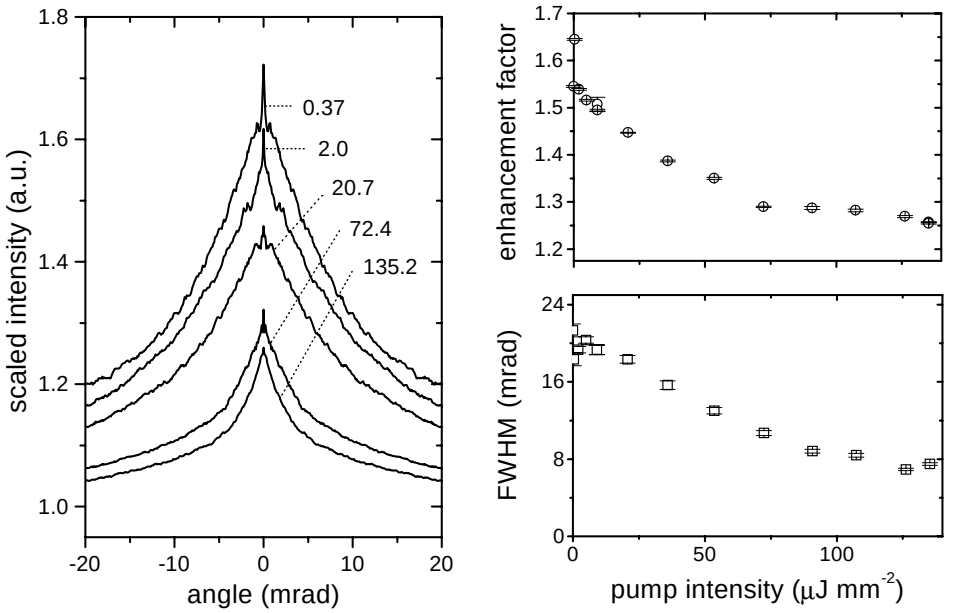

figure 4.9 *Enhanced backscattering cones of Kiton Red with $\ell = 3$ μm. In the left graph the pumping intensities (in μJ mm^{-2}) are indicated. In the right graphs the enhancement factor and the widths of the cones are shown.*

The backscattering cones are fitted with scaled diffusive cone shapes (figure 4.10). For low pumping intensities (left) the agreement is rather good, but it starts to deviate for higher intensities (from 35.9 μJ mm^{-2}). On the right it is evident that for small angle ϑ, there is no agreement at all. Long paths have become relatively more important than in the $\ell = 10$ μm samples.

This is made more clear when the tangents of the top angles Θ are plotted against the widths of the cones (figure 4.11). Figure 4.11a shows calculated values from diffusion theory with an inhomogeneous gain coefficient. It can be seen that the data points are not on a straight line as would have been the case for scaled diffusive cones. A straight line fit through the points at

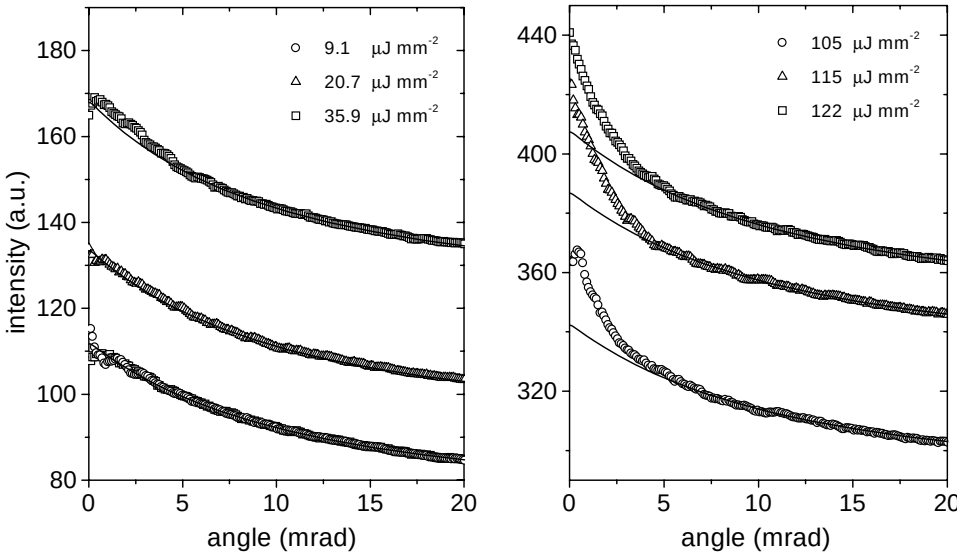

figure 4.10 *Backscattering cones (Kiton Red, $\ell = 3$ μm) of low pump intensity (left) and of high pump intensity (right) fitted with scaled and off-setted theoretical cones from diffusion theory (solid lines). In the left graph the two cones with the lowest pump intensities can be fitted well with cones from diffusion theory, in which no amplification is incorporated. The cone of 35.9 μJ mm^{-2} starts to deviate from the theoretical curve for small angles. On the right, the cone profiles at high pumping intensities can not be fitted with diffusive cones.*

large FWHM (low pumping intensities) does not intersect the origin. $-\tan\Theta$ in this region decreases faster than can be expected from normal diffusion, which means that the top angle is smaller than expected. At small FWHM the curve bends back to the origin, indicating that at very high inversion densities, the very long paths lose on importance relative to the shorter paths. This implies that average path lengths have become so long that most of them probe the system outside the amplifying volume. Their paths through the amplifying volume are on the average equal. These cones are still narrowed of course, since short paths within the gain volume are of minor importance. In the experimental data (figure 4.11b) a straight line fit also yields an intersection with the positive x axis. The bending back can not be observed since data points at very small widths are not experimentally achievable due to sample damage at high pump exposure.

In figure 4.12 we present an experimental cone at high pumping intensity, fitted with a theoretical cone shape as obtained from the procedure described in section 4.2. An inhomogeneous gain profile is calculated (solid line in figure 4.12, on the right) to which a rectangular box is modelled (dotted line). This rectangular profile is used in further calculations, described in [31]. Al-

though the agreement between experiment and theory can be made very good, the exact shape depends rather critically on parameters like the depth of the box and the gain length ℓ_g.

4.4 conclusions

We have observed the narrowing of enhanced backscattering cones of a random laser upon increasing the pumping intensity. The cone shapes of two different systems with $\ell = 10$ μm and $\ell = 3$ μm differ, in that they can not be scaled onto each other by adjusting the width and the enhancement factor. The peaks of the 3 μm samples are narrower than those of the 10 μm samples, indicating that long paths relatively have a higher importance in the 3 μm samples. Enhancement factors decrease as a result of an increasing background of spontaneaously emitted light and ASE, when the pumping intensity is increased.

The experimental cones can not be fitted with theoretical curves from [30] (homogeneous gain coefficient). All cones measured can be fitted when an inhomogeneous inversion profile is used in the calculations [31]. The predicted cone shapes, however, exhibit a very critical dependence on parameters like the gain length ℓ_g and the depth of the inversion profile.

No indication of a clear threshold-transition is present in our measurements of the widths and the enhancement factors of enhanced backscattering cones. This is not surprising, since the threshold states a condition for the amount of inversion that has to be present for light initiated by spontaneous emission, to alter its spectral properties. In our experiments, the light that is measured in the backscattering cone is not initiated inside the system, but originates from an external probe beam. It is therefore not required that a threshold found in the spectral width (chapter 2), will also be observable in the widths of the cones, or in their enhancement factors. However, the enhancement factors are related to the background value $\gamma_s + \gamma_d$, but the presence of probe light is expected to influence the threshold position (see for example [19] or injection locking experiments [5]).

Within the present experimental configuration, many properties could still be investigated. For example the dependence on the pumping beam diameter or on the intensity of the probe beam, could provide useful information on these systems. Time-resolved backscattering, which is not possible with the present setup, could prove a very powerful tool in investigating path length distributions of light in a random laser. These measurements also allow the mechanism of spectral narrowing (ch. 2) to be investigated in greater detail.

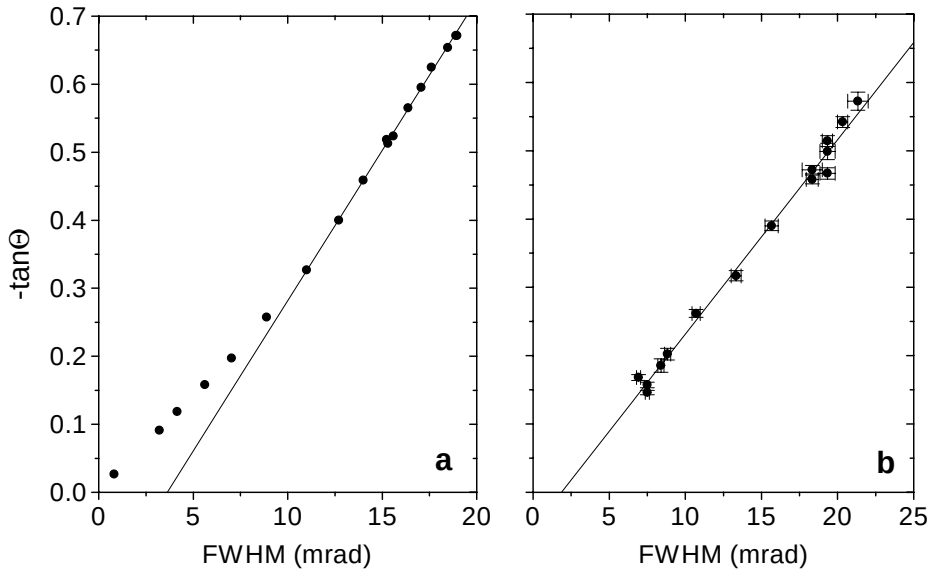

figure 4.11 *The tangent of the top angle* Θ *as a function of the width of the cone (*$\ell = 3\ \mu m$*). a) From diffusion theory with inhomogeneous gain profile (see section 4.2). b) for the experimental cones (the vertical scale should be multiplied by a factor 2). It is clear that* $\tan\Theta$ *of the experimental cones can not be fitted with diffusive cones with an effective transport mean free path, since this would result in an extrapolation through the origin. The theoretical cones in a) show the same behaviour. At small angles a curve that would connect all data points bends back to the origin. No experimental data is available for these small cone widths.*

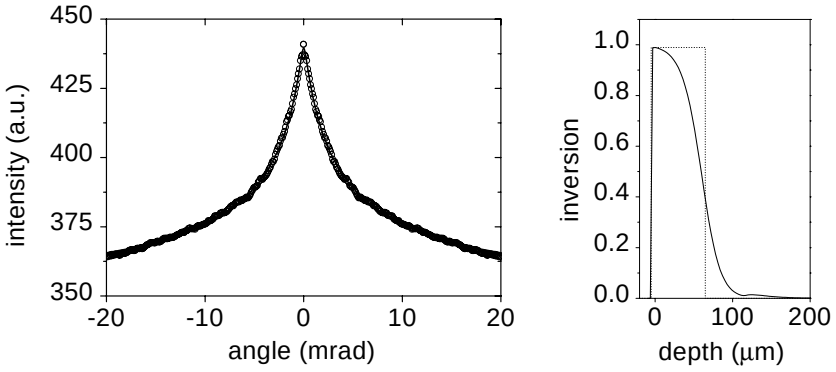

figure 4.12 *left: Backscattering cone (*$\ell = 4\ \mu m$*) at high pumping intensity (135* $\mu J\ mm^{-2}$*) fitted with a cone from diffusion theory including an inhomogeneous gain profile (see section 4.2). The quality of the fit is good. right: The inversion profile as found from [32] (solid line) and the square well by which it is modelled to facilitate calculations (dotted line). The fit on the left was obtained by using* $\ell_g = 200\ \mu m$ *and a inversion box depth of 20* μm*.*

epilogue

review and outlook

We have presented in this thesis a number of experiments shedding light on different aspects of random laser systems. We found that the laser threshold, which is very notably present in the spectral characteristics of a random laser, does not show up when we probe the system with an external beam. It might be possible that effects we expected to take place beforehand, like the change in intensity distribution in chapter 3, were obscured by other more important effects, like in this case the increase of background fluorescence. There is, however, a big difference between a pumped random laser and a random laser that is pumped and probed at the same time. In the first case all light is initiated by spontaneous emission and in the second case we have a large contribution of coherent stimulated emission. There is no compelling connection between the behaviour of the system in one case and the other. To be able to combine the observed effects into one picture, an accurate theory of the underlying dynamics is needed. This theory must be able to incorporate rate equations for the pumping intensity, fluorescence, and inversion population, together with diffusive transport of light and the propagation of coherent light from an external beam that is amplified and multiply scattered in the medium. Efforts in this direction are made at the moment by Gijs van Soest and Ad Lagendijk. Upshot of these investigations is for example that the 'photonic bomb' picture (more light generated in a certain volume than lost out of it by diffusion), that is usually connected to the threshold crossing is not correct. A detailed intuitive picture of the threshold dynamics is still lacking.

Also, from the experimental side, many further investigations could be done. A number of these possibillities are mentioned in the conclusions of the experimental chapters. Very interesting will be time resolved measurements, since traveled path lengths are then expressed by time delays. They, however, require very short laser pulse lengths and very fast detection hardware.

dankwoord

Er is een aantal mensen wie ik veel dank verschuldigd ben voor hun belangstelling en hulp tijdens mijn afstudeeronderzoek en bij het schrijven van deze scriptie, die inmiddels behoorlijk wat lijviger geworden is dan mijn afstudeerbegeleiders en ik zelf vooraf hadden voorzien.

Allereerst mijn begeleider en partner in crime wat betreft de random lasers, Gijs! van Soest, met wie ik een goede tijd heb gehad, zeker niet alleen in wetenschappelijk, maar ook in vriendschappelijk opzicht. Ik wil hem ook bedanken voor mijn inwijding in de muziek van een aantal alternatieve bands, die ik erg ben gaan waarderen. Gijs, veel succes in het laatste jaar van je promotie!

Ad Lagendijk, mijn andere scriptiebegeleider, wil ik bedanken voor mijn verblijf in zijn groep *Waves in Complex Media*. Zijn wetenschappelijke enthousiasme werkt enorm aanstekelijk en maakt van zijn onderzoeksgroep een ideale plaats om als student mee te draaien in de praktijk van succesvolle wetenschap.

Ik wil Dirk Riese bedanken voor de begeleiding van mijn Eigen Werk III en zijn nuchtere kijk op de dingen die we besproken tijdens onze ontelbare avonden in de mensa, dingen die af en toe voor mij waardevolle adviezen waren, ook wat betreft mijn afstudeerwerk.

Wim Koops wil ik bedanken voor alle onderdelen die hij gemaakt heeft voor de opstellingen die we gebruikt hebben tijdens mijn Eigen Werk III en IV. Natuurlijk is ook zijn humor niet weg te denken uit onze groep. Ik hoop dat zijn superieure klapschaats een commercieel succes wordt.

Mensen van de werkplaats wil ik bedanken voor de het maken van de samplehouders: Johan van de Ridder voor het teflon gedeelte, Bert Zwart voor de afdekglaasjes en Jan Mulder en Jan Dekker voor het vinden van goede lijm tussen de twee onderdelen, welke ook nog bestand moest zijn tegen methanol. Vaak moesten deze klusjes even snel tussen hun andere werk door. Ook Joost Overtoom en Flip de Leeuw wil ik bedanken, niet in de laatste plaats voor de niet aflatende stroom bier tijdens de lab-borrels.

Verder wil ik alle mensen bedanken die verantwoordelijk waren voor de goede sfeer in de groep: Martijn 'always on the move' Wubs, bij wie ik met al mijn theoretische vragen terecht kon, A. Femius Koenderink, die de zwaarste experimentele tegenvallers toch altijd weet te relativeren met zijn ongeëvenaarde humor, Frank Schuurmans, Denis Fenistein, avec qui on n'est jamais en mal d'un sujet de conversation, Jaime Gomez-Rivas, Lydia Bechger, Mischa Megens, met zijn enthousiasme en belangstelling voor alles wat er in de groep omging, Judith Wijnhoven, Michiel Thijssen, tegenwoordig mijn koorgenoot, Willem Vos, Arnout Imhof, Henry Schriemer, Rudolf Sprik, aan wie je werkelijk alle natuurkundige vragen kunt stellen en hij weet ze, Gerard Wegdam, Duong Hieu Dau en Henry van Driel. Zij allen maakten voor mij het lab een plaats waar ik graag kwam en die ik zeker zal missen.

Frank

references

[1] A.L. Schawlow and C.H. Townes, *Phys. Rev.* **112**, 1940 (1958)

[2] V.S. Letokhov, *Zh. eksp. i teor. fiz.* **4**, 477 (1965)

[3] D.S. Wiersma, M.P van Albada, and A. Lagendijk, *Nature* **373**, 203 (1995)

[4] D.S. Wiersma and A. Lagendijk, *Phys. Rev. E* **54**, 4256 (1996)

[5] R.M. Balachandran, A.E. Perkins, and N.M. Lawandy, *Opt. Lett.* **21**, 650 (1996)

[6] C. Gouedard et al., *J. Opt. Soc. Am. B* **10**, 2358 (1993)

[7] M. Siddique et al., *Opt. Lett.* **21**, 450 (1996)

[8] H.C. van de Hulst, *Light Scattering by Small Particles*, Dover Publications, New York (1957)

[9] B. Berne and R. Pecora, *Dynamic Light Scattering*, Wiley & Sons, New York (1976)

[10] M.B. van der Mark, *Propagation of Light in Disordered Media*, PhD. thesis (1990)

[11] P.N. den Outer, *Multiple Light Scattering in Random Discrete Media*, PhD. thesis (1995)

[12] R. Loudon, *The Quantum Theory of Light*, 2$^{\text{nd}}$ ed., Clarendon Press, Oxford (1983)

[13] *Lamdachrome Laser Dyes Handbook*, ed. by U. Brackman (1994)

[14] R.M. Balachandran, and N.M. Lawandy, *Opt. Lett.* **22**, 319 (1999)

[15] G. van Soest, M. Tomita, and A. Lagendijk, *Opt. Lett.* **24**, 306 (1999)

[16] R. Ambartsumyan, N.G. Basov, P.G. Kryukov, and V.S. Letokhov in *Progress in Quantum Electronics*, Pergamon, Oxford, pp.107-185 (1970)

[17] M.A. Noginov, H.J. Caulfield, N.E. Noginova, and P. Venkateswarlu, *Opt. Comm.* **118**, 430 (1995)

[18] G.A. Berger, M. Kempe, and A.Z. Genack, *Phys. Rev. E* **56**, 6118 (1997)

[19] F.J. Poelwijk, *Over de threshold-overgang in random lasers*, internal communication (2000)

[20] W.A. Kampfer, *Pigment Handbook (Patton) Vol. I*, Wiley, New York (1973)

[21] R.M. Balachandran, N.M. Lawandy, and J. A. Moon, *Opt. Lett.* **22**, 319 (1997)

[22] J.C. Dainty, *Laser Speckle and Related Phenomena*, Springer-Verlag, Berlin (1975)

[23] M. Minnaert, *De natuurkunde van 't vrije veld*, Thieme, Zutphen (1937)

[24] K.M. Watson, *J. Math. Phys.*, **10**, No. 4, 668 (1968)
[25] Y. Kuga and A. Ishimaru, *J. Opt. Soc Am.* **1**, 831 (1984)
[26] M.P. van Albada and A. Lagendijk, *Phys. Rev. Lett.* **55**, 2692 (1985)
[27] P.-E. Wolf and G. Maret, *Phys. Rev. Lett.* **55**, 2696 (1985)
[28] M.B. van der Mark, M.P van Albada, and A. Lagendijk,*Phys. Rev. B* **37**, 3575 (1988)
[29] E. Akkermans, P.-E. Wolf, and R. Maynard *Phys. Rev. Lett.* **56**, 1471 (1986)
[30] D.S. Wiersma, M.P van Albada, and A. Lagendijk, *Phys. Rev. Lett.* **75**, 1739 (1995)
[31] W. Deng, D.S. Wiersma, and Z.-Q. Zhang, *Phys. Rev. B* **56**, 178 (1997)
[32] K. Totsuka, G. van Soest, A. Lagendijk, and M. Tomita, accepted for publication *J. Appl. Phys.*
[33] A. Ishimaru, *Wave Propagation and Scattering in Random Media*, vol. 1, Academic Press, New York (1978)